Motion of charged particles in magnetic fields created by symmetric configurations of wires

Jacobo Aguirre*
Centro de Astrobiología, CSIC-INTA
28850 Torrejón de Ardoz (Spain)

Alejandro Luque†
Departament de Matemàtica Aplicada I
Universitat Politècnica de Catalunya
08028 Barcelona (Spain)

Daniel Peralta-Salas‡
Departamento de Matemáticas
Universidad Carlos III
28911 Leganés (Spain)

30th September 2009

*aguirreaj@inta.es
†alejandro.luque@upc.edu
‡dperalta@math.uc3m.es

Abstract

In this paper we study the motion of a charged particle in the presence of a magnetic field created by three different systems of wires: an infinite rectilinear filament, a circular wire and the union of both. In the first case we prove that the equations of motion are Liouville integrable and we provide a complete description of the trajectories, which turn out to be of helicoidal type. In the case of the circular wire we study some restricted motions and we show that there is a trapping region similar to the Van Allen inner radiation belt in the Earth magnetosphere. We prove the existence of quasi-periodic orbits using Moser's twist theorem, and the existence of scattering trajectories using differential inequalities. We also provide numerical evidence of Hamiltonian chaos and chaotic scattering by computing several Poincaré sections, Lyapunov exponents, fractal basins and their fractal dimensions. A similar study is done for the third system, although quasi-periodic orbits are proved to exist only under certain (perturbative) assumption. From the viewpoint of the applications we propose a magnetic trap based on these configurations. Furthermore, the circular wire system can be interpreted as a simplified model of the levitated magnetic dipole, one of the recent proposals to confine a hot plasma for fusion power generation, and hence our work provides a verification of confinement and quasi-periodicity, beyond the adiabatic approximation, for this plasma system. Apart from contributing to the rigorous theory of the motion of charges in magnetic fields, this paper illustrates that very simple magnetic configurations can give rise to complicated, even chaotic trajectories, thus posing the question of how the complexity of magnetic lines affects the complexity of particle motions.

Contents

1 Introduction

The study of the motion of a charged particle in a magnetic field has long been of interest in several areas of physics, as condensed matter theory [15, 33], accelerator physics [26], magnetobiology [19], magnetohydrodynamics [7], plasma physics [32, 35] and stellar astrophysics [31]. In general it is not possible to integrate analytically the equations of motion, and hence most of the literature makes use of numerical tools [43] or adiabatic approximations like the guiding centre [30, 40]. Regretfully, if we want to obtain global results (for all time) or the field is far from being uniform, the guiding centre approximation is of little help, as illustrated with some planar examples in [41]. Therefore, other techniques to study the qualitative properties of the motion must be introduced.

In spite of the importance of the previously mentioned contexts, there are not many rigorous results on the motion of charges in concrete magnetic fields. Of course, trajectories can be obtained explicitly in the special case of a uniform field [22], but this situation is rather exceptional. Even in the case of perturbations of uniform magnetic fields it is very hard to prove the existence of helicoidal trajectories, which has only been achieved for some particular

cases [12]. On the other hand, the Hamiltonian nature of the equations of motion (Newton-Lorentz equations) allows us to apply some techniques from Hamiltonian systems, as KAM theory or Moser's twist theorem. For example, the proof of the existence of quasi-periodic solutions in the presence of the magnetic field created by a dipole (Störmer problem) and other magnetic fields with rotational symmetry was first achieved by Braun in a remarkable paper [9], using Moser's twist theorem. Some refinements of this idea were applied to other axisymmetric magnetic fields in [13, 39] to cover some cases for which Braun's approach does not work.

Let us also mention that there is abundant literature on the motion of charged particles subjected to magnetic fields in closed Riemannian manifolds, e.g. [11] and references therein. These works are important in the context of differential geometry and dynamical systems, but they will not be helpful to us because we shall consider the physically realistic situation of motions in Euclidean space, paying attention to the sources of the fields.

In this paper we are interested in magnetic fields created by steady flows of electricity along several wires. This is a standard way of producing magnetic fields in physics and electrical engineering [24], and has the advantage that the field can be easily described in mathematical terms using the Biot-Savart law [22]. The topological structure (from the dynamical systems viewpoint) of magnetic fields created by current filaments can be very complicated. Some recent results on the existence of first integrals and chaos can be consulted in [2, 3, 17]. In this work we shall not study the magnetic lines (a static situation), but the motion of a charged particle in the presence of a magnetic field (a dynamical situation). Contrary to what happens in some plasma or force-free systems, where it is a good approximation to consider that particles follow magnetic lines [27, 32, 35], this is not the case here, and in fact we shall see that the particle trajectories and the lines of the field are usually completely different. In general the motion is described by a three degrees of freedom (3DOF) Hamiltonian system, which makes very complicated to understand the connection between the structure of the magnetic field and the trajectories of a charged particle.

Since the study of the motion for general configurations of wires is a formidable task, we shall focus on the following specific examples: motion in the presence of a rectilinear wire, a circular wire and the union of both. These are the simplest cases to consider, but we shall see that they exhibit very interesting dynamical properties, such as the existence of periodic and quasi-periodic solutions, scattering trajectories of helicoidal type and chaos. It is surprising to discover that, to the best of our knowledge, there is no detailed study of these systems in the literature, with the exception of the straight line wire for which a complete description was only given quite recently [42] (for partial results see [29]).

Let us summarise the main contributions of this work. On the one hand we study in detail and obtain new results, both analytically and numerically, on some elementary but realistic magnetic systems, thus filling a gap in the literature. Moreover, the circular wire can be interpreted as a simplified model of the levitated magnetic dipole system [23], one of the most recent proposals to confine a hot plasma for fusion power generation. Therefore, all our results on the motion of a charge in the magnetic field of a ring wire translate into this context, specifically

they provide a rigorous verification of the existence of confinement and quasi-periodic orbits for this kind of systems, beyond numerics and adiabatic approximation (the usual tools to analyse plasma confinement). On the other hand, concerning the relationship between the complexity of magnetic fields and the complexity of the motion, we provide numerical evidence that chaos can arise even for very simple and ordered magnetic configurations.

The contents of this paper are organised as follows. In Section 2 we introduce some notation and preliminaries. The motion in the presence of a rectilinear filament is considered in Section 3, where it is proved that all trajectories are of helicoidal type and asymptotically move in the same direction. This result was already obtained in [42], but we provide a more concise proof for the sake of completeness. In Section 4 we study the motion in the magnetic field of a circular wire. The main results that we obtain are the existence of a trapping region with quasi-periodic solutions (similar to the Van Allen inner radiation belt in the Earth magnetosphere [9]) and the presence of trajectories of certain type which escape to infinity. An application in the context of magnetic traps is also included. The coupled system (rectilinear and circular wires) is analysed in Section 5, where we show the existence of a trapping region and quasi-periodic trajectories under certain assumptions. In Section 6 we perform an extensive numerical study of these systems, computing several Poincaré sections and Lyapunov exponents to illustrate the presence of chaos. The chaotic scattering is also analysed by computing the fractal basins and their fractal dimensions, thus showing the complex behaviour of the solutions which escape to infinity. A final section is included to state some open problems and future lines of research.

2 Notation and preliminaries

We consider the ambient space $\mathbb{R}^3$ endowed with the standard inner product $\cdot$, vector product $\wedge$ and Euclidean norm $|\cdot|$. In this paper an electric wire will be represented by a smooth curve $L \subset \mathbb{R}^3$ and a constant J which stands for the current intensity. If $l : \tau \in [a,b] \subset \mathbb{R} \longmapsto l(\tau) \in \mathbb{R}^3$ is a parametrisation of the curve L, then the magnetic field B created by the wire (L,J) at the point $q \in \mathbb{R}^3$ is given by the Biot-Savart law,

$$B(q) = \frac{\mu_0 J}{4\pi} \int_a^b \frac{l'(\tau) \wedge (q - l(\tau))}{|q - l(\tau)|^3} d\tau, \tag{1}$$

where μ_0 denotes the magnetic permeability constant. It is standard that the vector field B does not depend on the parametrisation of L. According to the superposition principle the magnetic field created by n wires $(L_1, J_1), \ldots, (L_n, J_n)$ is given by the sum $B = \sum_{i=1}^n B_i$ of the individual magnetic fields B_i. For the sake of simplicity we will set $\mu_0/4\pi = 1$ all along this paper.

It is well known that B is a divergence free vector field, analytic in the complement of the current distribution. Following the standard terminology of electromagnetism, we call *magnetic lines* to the integral curves of B and *magnetic surface* to a surface which is covered by magnetic lines.

The equations of motion of a (non-relativistic) unit-mass, unit-charge particle in the presence of a magnetic field B are given by the Newton-Lorentz law:

$$\ddot{q} = \dot{q} \wedge B(q), \tag{2}$$

where the dot over q denotes, as usual, the time derivative. This equation can be written equivalently in a Hamiltonian way whenever there is a globally defined vector potential A such that $B = \operatorname{rot} A$. If this is the case, the Hamiltonian function is $H(q,p) := \frac{1}{2}(p - A(q))^2$. In all the examples considered in this paper the vector potential A is globally defined (in the complement of the wires) because $\int_S B \cdot \nu d\Sigma = 0$ for any closed surface $S \subset \mathbb{R}^3 \setminus \bigcup L_i$, where ν is the outward unit normal to S and $d\Sigma$ is the standard area measure of S.

A particle trajectory $q(t)$ is called of *scattering type* if $\lim_{t\to\infty} |q(t)| = \infty$. A particular kind of scattering trajectory $q(t)$ is called *helicoidal* if there is a unit vector n and constants $A > 0$ and B such that $q_{||}(t) := n \cdot q(t)$ verifies $q_{||}(t) \geq At + B$ for all $t \geq 0$, and $q_\perp(t) := q(t) - q_{||}(t)$ is periodic. This definition was introduced in [12] with the more restrictive assumption that $\dot{q}_{||}(t)$ is constant. As this hypothesis is not generally fulfilled we have decided to drop it. It is clear that the image of $q(t)$ in $\mathbb{R}^3$ for $t \geq 0$ resembles a "deformed helix" with axis in the n direction.

We will denote by $(r, \phi, z) \in \mathbb{R}^+ \times \mathbb{S}^1 \times \mathbb{R}$ the standard cylindrical coordinates in $\mathbb{R}^3$, and by $\{\partial_r, \partial_\phi, \partial_z\}$ its associated orthogonal basis of vector fields. Here $\mathbb{R}^+$ stands for $[0, \infty)$. Remember that $|\partial_r| = |\partial_z| = 1$ and $|\partial_\phi| = r$. We will make extensive use of this coordinate system in what follows.

As usual $K(k)$ and $E(k)$, $k \in [0, 1)$, are the *complete elliptic integrals* [1] defined by:

$$K(k) := \int_0^{\frac{\pi}{2}} \frac{d\theta}{\sqrt{1 - k\sin^2(\theta)}}, \qquad E(k) := \int_0^{\frac{\pi}{2}} \sqrt{1 - k\sin^2(\theta)}\, d\theta\,.$$

Let us summarise some properties of the complete elliptic integrals which will be used in forthcoming sections:

1. $K(0) = E(0) = \pi/2$.
2. $\lim_{k\to 1^-} K(k) = \infty$, $\lim_{k\to 1^-} E(k) = 1$.
3. $\frac{dK(k)}{dk} = \frac{E(k)}{2k(1-k)} - \frac{K(k)}{2k}$, $\qquad \frac{dE(k)}{dk} = \frac{E(k)-K(k)}{2k}$.
4. $K(k) = \frac{\pi}{2}(1 + \frac{k}{4} + \frac{9k^2}{64} + O(k^3))$, $\quad E(k) = \frac{\pi}{2}(1 - \frac{k}{4} - \frac{3k^2}{64} - O(k^3))$, $\quad$ for $k \simeq 0$.

3 Motion in the magnetic field of an infinite rectilinear wire

Let $\mathcal{R}$ be an infinite rectilinear filament carrying a current of intensity $J_\mathcal{R}$. The Cartesian coordinates can be chosen in such a way that $\mathcal{R}$ is given by the z-axis, and the current is flowing in

the positive direction, so that $J_{\mathcal{R}} > 0$. The magnetic field created by this wire is given by the following expression [22]:

$$B_{\mathcal{R}} = \frac{2J_{\mathcal{R}}}{r^2}\partial_\phi \,.$$

It is clear that this vector field has the symmetries $S_1 = \partial_z$ (translation) and $S_2 = \partial_\phi$ (rotation), and hence the integral curves of $B_{\mathcal{R}}$ are circles around the z-axis.

We are interested in the motion of a unit-charge, unit-mass particle subjected to the magnetic field $B_{\mathcal{R}}$. The interest of this problem lies in the fact that it is a physically meaningful 3DOF Hamiltonian system which can be integrated by quadratures, a rather unusual property. Surprisingly, the only reference that we have found where this system is studied in detail is quite recent [42]. For the sake of completeness we will provide a more explicit proof of the main results in [42], emphasising the integrability of the motion. This system is also studied in [29], but only partial results concerning the motion in the r coordinate are obtained.

Let us see that the Euclidean symmetries give rise to two independent first integrals of the motion, thus allowing us to obtain a complete qualitative description of the particle trajectories. There is no loss of generality in assuming that $2J_{\mathcal{R}} = 1$, otherwise the equations are reduced to this case just doing the time-scaling $\tilde{t} := 2J_{\mathcal{R}}t$. Then, Newton-Lorentz Eqs. (2) in cylindrical coordinates read as:

$$\ddot{r} - r\dot{\phi}^2 = -\frac{\dot{z}}{r}\,, \tag{3}$$

$$r^2\ddot{\phi} + 2r\dot{r}\dot{\phi} = 0\,, \tag{4}$$

$$\ddot{z} = \frac{\dot{r}}{r}\,. \tag{5}$$

As usual, the kinetic energy $E := \frac{1}{2}(\dot{r}^2 + r^2\dot{\phi}^2 + \dot{z}^2)$ is a conserved quantity of this system. Furthermore, integrating Eqs. (4) and (5) we get two additional first integrals of the motion, the generalized angular and linear momenta:

$$L := r^2\dot{\phi}\,, \tag{6}$$

$$P := \dot{z} - \ln r\,. \tag{7}$$

Therefore the motion is restricted to the level sets $\{E = E_0, L = L_0, P = P_0\}$ for constants $E_0, L_0, P_0 \in \mathbb{R}$ determined by the initial conditions. Writing the first integrals in phase space coordinates $(r, \phi, z, p_r, p_\phi, p_z)$ we have $E = \frac{1}{2}p_r^2 + \frac{1}{2r^2}p_\phi^2 + \frac{1}{2}(p_z + \ln r)^2$, $L = p_\phi$ and $P = p_z$. It is readily checked that these functions are in involution and almost everywhere independent, so the system is Liouville integrable. Let us now integrate it by quadratures.

Using Eqs. (6) and (7) we can eliminate the dependence on the coordinates ϕ and z in Eq. (3), thus reducing the motion to an equation in the r coordinate:

$$\frac{1}{2}\,\dot{r}^2 + U(r) = E_0\,, \tag{8}$$

where the effective potential $U(r)$ is

$$U(r) := \frac{L_0^2}{2r^2} + \frac{(P_0 + \ln r)^2}{2}\,.$$

It is easy to check that $\lim_{r\to 0^+} U(r) = \lim_{r\to\infty} U(r) = \infty$, and that $U(r)$ has a unique global minimum r_m and a unique inflection point $r_i > r_m$. This implies that all the solutions $r(t)$ to Eq. (8) are periodic. The period of each solution depends on the constants E_0, L_0 and P_0, and is defined by a smooth function $T_0 := T(E_0, L_0, P_0)$, which can be extended smoothly to the constant solutions $r(t) = r_m$.

Since the coordinate r is always bounded we get that a solution to Eqs. (3), (4) and (5) is bounded if and only if the coordinate z is. If $r(t)$ is a solution to Eq. (8), we can integrate Eqs. (6) and (7) to yield

$$\phi(t) = \phi_0 + \int_0^t \frac{L_0 dt}{r^2(t)}\,,$$
$$z(t) = z_0 + P_0 t + \int_0^t \ln r(t) dt\,.$$

As $r(t)$ is a periodic function of period T_0, it is standard that the following identity holds

$$\int_0^t \ln r(t) dt = \mu_0 t + G(t)\,,$$

where $\mu_0 := \frac{1}{T_0}\int_0^{T_0} \ln r(t) dt$ and $G(t)$ is a periodic function of (not necessarily minimal) period T_0. Note that μ_0 is a smooth function of E_0, L_0, P_0 because T_0 and $r(t)$ depend smoothly on the constants of motion. Accordingly, the solution $z(t)$ is bounded if and only if the equation

$$P_0 + \mu_0 = 0$$

holds in the space of parameters (E_0, L_0, P_0).

Lemma 3.1. *For any values of the constants of motion (E_0, L_0, P_0), with $E_0 \neq 0$, we have that*

$$P_0 + \mu_0 > 0$$

.

Proof. First let us observe that this inequality is straightforward if $r(t)$ is a constant solution of Eq. (8), given by $r(t) = r_m$ and $E_0 = \frac{L_0^2}{2r_m^2} + \frac{L_0^4}{2r_m^4}$. In this case, as $E_0 \neq 0$ implies that $L_0 \neq 0$, we have that

$$P_0 + \mu_0 = P_0 + \ln r_m = \frac{L_0^2}{r_m^2} > 0\,.$$

Otherwise, let t_- and t_+ be the time values where the solution $r(t)$ reaches its minimum and maximum respectively, assuming that $0 \leq t_- < t_+ < T_0$. Then, using that $r(t)$ satisfies the Newtonian equation $\ddot{r} = \frac{L_0^2}{r^3} - \frac{P_0 + \ln r}{r}$ associated to Eq. (8), we write $P_0 + \mu_0$ as

$$\frac{2}{T_0} \int_{t_-}^{t_+} \Big[\frac{L_0^2}{r(t)^2} - r(t)\ddot{r}(t) \Big] dt \, .$$

Integrating by parts the second summand of the integral above, and taking into account that $\dot{r}(t_-) = \dot{r}(t_+) = 0$ we finally conclude that

$$P_0 + \mu_0 = \frac{2}{T_0} \int_{t_-}^{t_+} \Big[\frac{L_0^2}{r(t)^2} + \dot{r}(t)^2 \Big] dt > 0 \, ,$$

as we wanted to prove. □

This lemma implies that the coordinate $z(t)$ grows linearly in t when $t \to \infty$ and hence all the particle trajectories move in the positive z-axis direction after some transient of time no bigger than T_0. Consequently, if the angular momentum $L_0 \neq 0$, for every initial condition there exists $t_* \leq T_0$ such that for $t \geq t_*$ the trajectory of the corresponding charged particle moving under the action of $B_{\mathcal{R}}$ is helicoidal: periodic in the r-coordinate, linearly increasing in the z-coordinate (unbounded) and turning around the z-axis. Let us remark that the motion in the coordinate space is confined to the region enclosed by two cylinders of radii $r(t_-)$ and $r(t_+)$ respectively, which depend on the constants E_0, L_0, P_0. If $L_0 = 0$ the solution has no angular velocity, i.e. $\dot{\phi} = 0$, and the motion takes place on a half-plane $\phi = \phi_0$ determined by the initial condition. In this case, the initial condition $r_0 = \mathrm{e}^{-P_0}$ corresponds to an equilibrium solution, i.e. $E_0 = 0$.

Helicoidal motions with $\ddot{z} = 0$ were also obtained in [12] studying perturbations of uniform magnetic fields. The main difference is that the helicoidal trajectories in system $\mathcal{R}$ are oscillating because $\dot{z}$ does not need to be positive for all $t \geq 0$ (the constant $P_0 + \mu_0$ is perturbed by a periodic function which changes its sign). In Fig. 1 we have represented some trajectories in $\mathbb{R}^3$ to illustrate the different possible behaviours.

4 Motion in the magnetic field of a circular wire

The flow of electric current along a closed filament is one of the simplest ways to generate a magnetic field. In this section we provide a detailed analytical study of the motion of charges in the magnetic field of a circular wire, a system which has been very poorly studied in the literature in spite of its importance for applications. For example, let us mention that this system provides a toy model for the so called levitated magnetic dipole [23], a device to confine a hot plasma for fusion power generation. All our results can then be interpreted in this context.

First, in Section 4.1 we describe the magnetic field and the equations of motion, showing the existence of an additional first integral. Some 1-dimensional and 2-dimensional restricted

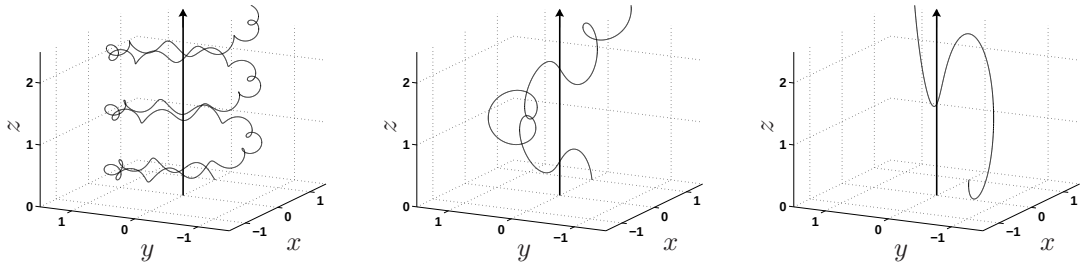

(a) $\dot{z}_0 = 0$ (b) $\dot{z}_0 = 0.5$ (c) $\dot{z}_0 = -0.5$

Figure 1: Particle trajectories of helicoidal type around an infinite rectilinear wire. The initial conditions are $r_0 = 1$, $z_0 = 0$, $\phi_0 = 0$, $\dot{r}_0 = 0.1$, $\dot{\phi}_0 = 0.1$. For clarity, the direction of the current is marked with an arrow in all pictures.

motions are studied in Section 4.2. In Section 4.3 we prove the existence of trapping regions of toroidal shape, which are similar to the plasma confinement regions in a levitated magnetic dipole, and the presence of quasi-periodic solutions in these domains. The technique of proof is adapted from [9] and consists in applying Moser's twist theorem after some manipulations of the Hamiltonian. These trapping regions have similar properties to the Van Allen inner radiation belt in the Earth magnetosphere, which suggests the application of this system to construct a magnetic trap, a possibility which is discussed in Section 4.4. Finally, in Section 4.5 we prove the existence of trajectories escaping to infinity.

4.1 Preliminary results

Without loss of generality one can assume that $\mathcal{C}$ is a circular filament defined by the coordinates $(r = 1, z = 0)$ and carrying a current of intensity $J_{\mathcal{C}} > 0$ in the direction of the vector field ∂_ϕ. The magnetic field created by this wire can be explicitly written in terms of the complete elliptic integrals $K(k)$ and $E(k)$, cf. Section 2, as follows:

$$B_{\mathcal{C}} = \frac{J_{\mathcal{C}} \partial_z I(r,z)}{r}\, \partial_r - \frac{J_{\mathcal{C}} \partial_r I(r,z)}{r}\, \partial_z \,, \tag{9}$$

where $I(r,z)$ is defined as

$$I(r,z) := -\sqrt{(1+r)^2+z^2}\Big[(2-k^2)K(k^2) - 2E(k^2)\Big]\,, \tag{10}$$

$$k^2 := \frac{4r}{(1+r)^2+z^2}\,. \tag{11}$$

This formula for the magnetic field of a circular wire is obtained taking into account that the vector potential $A = A_\phi(r,z)\partial_\phi$ is related to $I(r,z)$ as $I(r,z) = -r^2 A_\phi(r,z)$, where the expression of $A_\phi(r,z)$ is the one shown in [22]. Note that $B_\mathcal{C}$ is an analytic vector field in $\mathbb{R}^3\backslash\mathcal{C}$.

It is easy to check that the angle ϕ and the function $I(r,z)$ are first integrals of $B_\mathcal{C}$. In the following lemma we provide a topological characterization of the level sets of $I(r,z)$.

Lemma 4.1. *The level sets $I^{-1}(c) \subset \mathbb{R}^+ \times \mathbb{R}$ are diffeomorphic to $\mathbb{S}^1$ around the point $(r=1, z=0)$ for $c \in (-\infty, 0)$ and the only degenerate level is $I^{-1}(0) = \{r = 0\}$. The corresponding surfaces in $\mathbb{R}^3$ are revolution tori.*

Proof. First, we observe that $B_\mathcal{C} \neq 0$ at every point, which implies via Eq. (9) that $\nabla I \neq 0$ in $\mathbb{R}^+\backslash\{0\} \times \mathbb{R}$. In addition, we note that $k^2 \in [0,1]$ for any $(r,z) \in \mathbb{R}^+ \times \mathbb{R}$ and that $\nabla I = 0$ on the line $\{r = 0\}$.

From Property 2 in Section 2 and $k^2(\mathcal{C}) = 1$ it follows that $\lim_\mathcal{C} I(r,z) = -\infty$, thus implying that the level sets of I near $\mathcal{C}$ are closed curves. Using $\lim_\infty k^2 = \lim_{r\to 0} k^2 = 0$ and the Taylor series $(2-k^2)K(k^2) - 2E(k^2) = \pi/16 k^4 + O(5)$ around $k = 0$ (use the expansions given in Property 4 of Section 2) we get $\lim_{r\to\infty} I(r,z) = \lim_{r\to 0} I(r,z) = 0$. Let us now prove that $I(\mathbb{R}^+\backslash\{0\} \times \mathbb{R}) < 0$. On account of Eq. (10) it is enough to show that $(2-k)K(k) - 2E(k) > 0$ for $k > 0$. Indeed, from the definitions of $K(k)$ and $E(k)$, cf. Section 2, we obtain

$$(2-k)K(k) - 2E(k) = -k\int_0^{\pi/2} \frac{\cos(2\theta)d\theta}{\sqrt{1-k\sin^2\theta}} =$$
$$-k\left(\int_0^{\pi/4} \frac{\cos(2\theta)d\theta}{\sqrt{1-k\sin^2\theta}} + \int_0^{\pi/4} \frac{\cos(\pi-2\theta)d\theta}{\sqrt{1-k\cos^2\theta}}\right).$$

Since $\frac{\cos(2\theta)}{\sqrt{1-k\sin^2\theta}} < -\frac{\cos(\pi-2\theta)}{\sqrt{1-k\cos^2\theta}}$ for $\theta \in [0, \pi/4)$ the claim follows, thus establishing that all the regular level sets of $I(r,z)$ are compact, so they are closed curves. It is clear that if we consider also the angular variable ϕ these sets become revolution tori. □

A straightforward consequence of Lemma 4.1 is that the integral curves of $B_\mathcal{C}$ are circles around $\mathcal{C}$ except for the z-axis, which is a magnetic line oriented in the positive direction.

Next we describe the equations of motion for a charged particle moving under the action of $B_\mathcal{C}$. Unless otherwise stated, we shall assume in all this section that $J_\mathcal{C} = 1$ because we can always reduce to this case by doing the scaling of time $\tilde{t} := J_\mathcal{C} t$. Accordingly, the Newton-Lorentz equations of motion of a unit-mass, unit-charge particle subjected to the magnetic field $B_\mathcal{C}$, written in terms of $I(r,z)$, are the following:

$$\begin{aligned}
&\ddot{r} - r\dot{\phi}^2 = -\dot{\phi}\partial_r I(r,z)\,,\\
&r^2\ddot{\phi} + 2r\dot{r}\dot{\phi} = \dot{z}\partial_z I(r,z) + \dot{r}\partial_r I(r,z)\,,\\
&\ddot{z} = -\dot{\phi}\partial_z I(r,z)\,.
\end{aligned} \tag{12}$$

The kinetic energy $E := \frac{1}{2}(\dot{r}^2 + r^2\dot{\phi}^2 + \dot{z}^2)$ is a conserved quantity of this system of equations. Furthermore there is a second first integral (generalized angular momentum) which can be obtained integrating Eq. (12):

$$L := r^2\dot{\phi} - I(r,z)\,.$$

The initial conditions provide a value L_0 for this constant of motion, and therefore, proceeding in the standard way, we can reduce the equations of motion to a two degrees of freedom (2DOF) Hamiltonian system defined on the half-plane $(r,z) \in \mathbb{R}^+ \times \mathbb{R}$, whose Hamiltonian function is:

$$H(r,z,p_r,p_z) := \frac{1}{2}(p_r^2 + p_z^2) + V(r,z)\,, \tag{13}$$

with

$$V(r,z) := \frac{(L_0 + I(r,z))^2}{2r^2} \tag{14}$$

playing the role of an effective potential energy of the problem. The motion in the physical space $\mathbb{R}^3$ is obtained from solutions $(r(t), z(t))$ of this 2DOF Hamiltonian system just integrating the first order differential equation:

$$\dot{\phi} = \frac{L_0 + I(r(t),z(t))}{r(t)^2}\,.$$

Hamilton's equations of motion associated to the Hamiltonian function (13) read as follows:

$$\begin{aligned}
&\dot{r} = p_r\,, \qquad \dot{p}_r = \frac{(L_0 + I(r,z))^2}{r^3} - \frac{(L_0 + I(r,z))\partial_r I(r,z)}{r^2}\,,\\
&\dot{z} = p_z\,, \qquad \dot{p}_z = -\frac{(L_0 + I(r,z))\partial_z I(r,z)}{r^2}\,.
\end{aligned}$$

Our goal in the following sections is to provide a rigorous qualitative study of these equations, in particular to prove the existence of periodic, quasi-periodic and scattering motions. In spite of the simplicity of this system it contains some features of non integrability and chaos, as will be illustrated with numerical studies in Section 6.

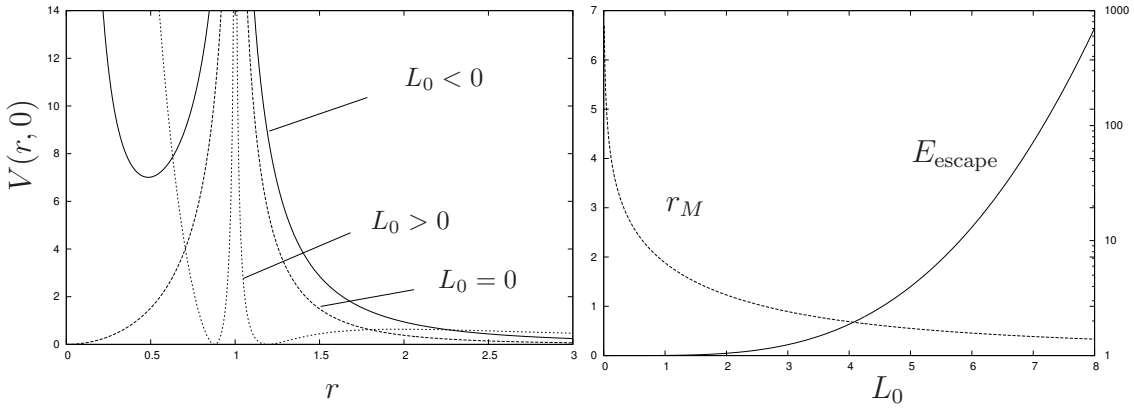

(a) (b)

Figure 2: (a): Sections at $z = 0$ of the potential $V(r, z)$ with $L_0 = -1, 0, 4$. (b): We plot the position of the saddle point r_M (logarithmic scale in the right axis), obtained from Eq. (17), and its corresponding escape energy $E_{\text{escape}} = V(r_M, 0)$ (left axis), as a function of L_0.

4.2 Some particular motions: trajectories on the invariant plane

A simple computation shows that the restriction of $B_{\mathcal{C}}$ (cf. Eq. (9)) to the z-axis looks as

$$B_{\mathcal{C}}|_{r=0} = \frac{2\pi}{(1+z^2)^{3/2}}\partial_z,$$

which readily implies that a particle with initial condition on the z-axis and initial velocity $\dot{z}_0$ tangent to this axis, has the equation of motion $\ddot{z} = 0$, and so it moves freely along the z-axis. In the standard terminology of mechanics it is said that the z-axis is an invariant set of the Newton-Lorentz equations of motion [16].

On the other hand, it is also ready to check that $B_{\mathcal{C}}|_{z=0}$ is orthogonal to the plane $\{z = 0\}$. Indeed an easy computation using that $\partial_z k(r, 0) = 0$ implies that $\partial_z I(r, 0) = 0$, and the result follows from Eq. (9). Hence, we have that $\{z = 0\} \subset \mathbb{R}^3$ is also an invariant set of the motion. In the phase space (r, z, p_r, p_z) this is equivalent to the invariance of the plane $\{z = 0, p_z = 0\}$ under the Hamiltonian vector field defined by Eq. (13). In this section we shall focus on studying the motion on this invariant plane, which will provide a first understanding of Hamilton's equations associated to Eq. (13).

The reduced motion on $\{z = 0, p_z = 0\}$ is described by the following 1DOF Hamiltonian system:

$$H(r, p_r) = \frac{1}{2}p_r^2 + W(r)\,, \tag{15}$$

with $W(r) := V(r,0) = \frac{[L_0+I(r,0)]^2}{2r^2}$, and hence the qualitative study of the solutions to the corresponding Hamilton's equations can be made through the analysis of the effective potential. The following lemma provides a full description of $W(r)$ in terms of the parameter L_0.

Lemma 4.2. *The function $W(r)$ is analytic in $(0,1)\cup(1,\infty)$ and satisfies these properties:*

1. $W(r) \geq 0$ *for any* L_0.
2. $\lim_{r\to 1^\pm} W(r) = \infty$ *and* $\lim_{r\to\infty} W(r) = 0$ *for any* L_0.
3. $\lim_{r\to 0^+} W(r) = \infty$ *if* $L_0 \neq 0$ *and* $\lim_{r\to 0^+} W(r) = 0$ *for* $L_0 = 0$.
4. *If $L_0 > 0$, $W(r)$ has two local minima at $0 < r_{m_1} < 1$ and $r_{m_2} > 1$ of value 0 and one local maximum at $r_M > r_{m_2}$. $W(r)$ has neither local maxima nor minima if $L_0 = 0$ (except at $r = 0$), and when $L_0 < 0$ it has only one local minimum at $r_m < 1$ of positive value and no local maxima. This structure is illustrated in Fig. 2(a) for some particular cases.*
5. *The escape energy is defined when $L_0 > 0$ as $E_{\text{escape}} := W(r_M) = V(r_M, 0)$. The maximum point r_M is decreasing with L_0, while E_{escape} is increasing, see Fig. 2(b).*

Proof. Using the definition of $W(r)$ and Lemma 4.1 it is easy to show that Properties 1, 2 and 3 hold. To prove Property 4 we compute the derivative of $W(r)$, which is

$$W'(r) = \frac{(L_0 + I(r,0))(r\partial_r I(r,0) - I(r,0) - L_0)}{r^3},$$

and study its zeros. If $L_0 > 0$ the local minima r_{m_1} and r_{m_2} are given by $L_0 + I(r,0) = 0$, while the local maximum verifies the equation $r\partial_r I(r,0) - I(r,0) = L_0$. When $L_0 < 0$ the function $L_0 + I(r,0)$ is strictly negative and $r\partial_r I(r,0) - I(r,0) - L_0 = 0$ has one solution at $r_m < 1$, see the graph of the function $r\partial_r I(r,0) - I(r,0)$ in Fig. 3(a). In the case $L_0 = 0$, $W'(r) \neq 0$ for $r > 0$ and $W(0) = W'(0) = 0$. Finally note from Fig. 3(a) that the radius r_M solving equation $r_M\partial_r I(r_M,0) - I(r_M,0) = L_0$ is decreasing with L_0 (the same happens with r_m). Moreover $|\partial_r I(r,0)|$ is decreasing with r provided that $r > 1$ (cf. Fig. 3(b)) and hence the escape energy $E_{\text{escape}} = \frac{[\partial_r I(r_M,0)]^2}{2}$ is decreasing with r_M, so increasing with L_0 whenever $L_0 > 0$. □

This lemma allows us to describe the solutions $(r(t), p_r(t))$ of the 1DOF Hamiltonian system (15), and integrating the equation

$$\dot{\phi} = \frac{L_0 + I(r(t),0)}{r(t)^2},$$

one easily obtains the motion on the plane $\{z = 0\}$. Let us summarise the main features of this motion which are obtained as a straightforward application of Lemma 4.2. The most relevant consequence is the existence of periodic, quasi-periodic and scattering trajectories of particles when moving on the invariant plane with energy H_0 and initial condition r_0.

1. If $L_0 > 0$ and $r_0 < 1$, then the solution $r(t)$ is periodic of period $T(H_0)$ and there exist constants $0 < r_1 < r_2 < 1$ such that $r_1 \leq r(t) \leq r_2$. This implies that the motion on the plane $\{z = 0\}$ is periodic or quasi-periodic depending on whether $2\pi/T(H_0)$ is rational or not.

2. If $L_0 > 0$ and $r_0 > 1$ we distinguish among several cases. If $H_0 < E_{\text{escape}}$ and $r_0 < r_M$ the solution $r(t)$ is periodic, while if $r_0 > r_M$ the solution is unbounded (scattering orbit). If $H_0 > E_{\text{escape}}$ the solution $r(t)$ is unbounded for any initial condition, that is why $W(r_M)$ is called escape energy. In the limit case $H_0 = E_{\text{escape}}$ there are 3 solutions: an unstable constant solution at $r = r_M$, a bounded solution which accumulates over $r = r_M$ and a scattering trajectory. For any values of H_0 and r_0 it holds that $r(t) > 1$. The unstable constant solution $r(t) = r_M$ for $H_0 = E_{\text{escape}}$ gives rise to an unstable periodic motion on $\{z = 0\}$. The other solutions provide periodic, quasi-periodic and scattering motions on the invariant plane.

3. If $L_0 = 0$ and $r_0 < 1$ then the solution $r(t)$ is periodic for any value of H_0. On the other hand, if $r_0 > 1$ the solution $r(t)$ is unbounded. This fact provides periodic, quasi-periodic and unbounded motions on the invariant plane.

4. If $L_0 < 0$ and $r_0 < 1$, the solutions $r(t)$ are periodic of period $T(H_0)$ and verify $0 < r(t) < 1$ for any H_0. In fact there is a stable constant solution $r(t) = r_m$ when $H_0 = W(r_m) > 0$, which provides a periodic motion on $\{z = 0\}$. The other periodic solutions provide periodic motions on the plane $\{z = 0\}$ if $2\pi/T(H_0)$ is rational, and quasi-periodic otherwise. Finally, if $r_0 > 1$ all the solutions escape to infinity, thus giving rise to scattering trajectories on the invariant plane.

Next we show that the invariant plane $\{z = 0\}$ is unstable. Indeed, taking into account that $\partial_z I(r, 0) = 0$, cf. Section 4.1, the potential $V(r, z)$ in Eq. (14) admits the Taylor expansion $V(r, z) = W(r) + \frac{F(r)}{2} z^2 + O(z^3)$, with

$$F(r) := \frac{1}{r^2}(L_0 + I(r, 0))\partial_{zz} I(r, 0)\,.$$

The Newton-Lorentz equation for the variable z is hence $\ddot{z} = -F(r)z + O(z^2)$, which at first order in z is an equation of harmonic oscillator type. This implies that the normal variational equation around a periodic solution $r(t)$ of Eq. (15) reads as

$$\ddot{z} = A(t)z\,, \tag{16}$$

where $A(t) := -F(r(t))$ is a periodic function of period T. Since $\partial_{zz} I(r, 0) = r\partial_z B_r(r, 0)$ on account of Eq. (9), and $B_r(r, z) < 0$ if $z < 0$ and $B_r(r, z) > 0$ if $z > 0$, it easily follows that $\partial_{zz} I(r, 0) \geq 0$. Therefore, whenever $L_0 \leq 0$, we have that $A(t) \geq 0$, and hence it is clear that the constant solution $z = 0$ to Eq. (16) is unstable. If $L_0 > 0$ the function $A(t)$ has no

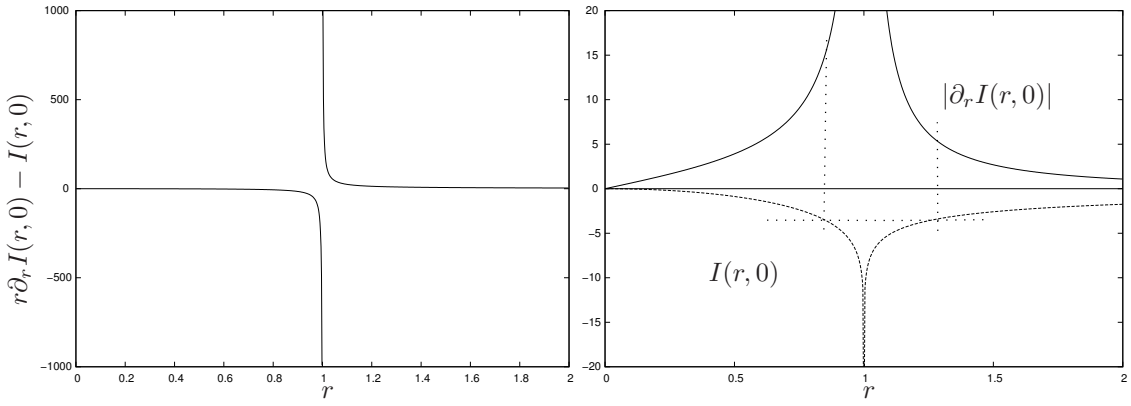

(a) (b)

Figure 3: (a) Graph of the function $r\partial_r I(r,0) - I(r,0)$ with respect to r. (b) Graph of the functions $|\partial_r I(r,0)|$ (upper plot) and $I(r,0)$ (lower plot). Dotted lines are plotted to show that $|\partial_r I(r,0)|$ is different for the two values of r that solve the equation $I(r,0) + L_0 = 0$. For the sake of completeness let us observe that $\partial_r I(r,0) = |\partial_r I(r,0)|$ for $r > 1$, and $\partial_r I(r,0) = -|\partial_r I(r,0)|$ if $r < 1$.

constant sign (however it can be proved that $\int_0^T A(t)dt > 0$), and we have not been able to prove instability although this is confirmed by numerical computations.

Summarising, we conclude that (because of instabilities) the motion restricted to the invariant plane $\{z = 0\}$ does not provide a qualitative picture of the dynamics in a nearby region of this plane. Accordingly, we need to look for stable invariant sets admitting a good perturbation behaviour to prove the existence of bounded and quasi-periodic motions. This is the goal of the next section.

4.3 Existence of quasi-periodic solutions

In this section we shall prove the existence of quasi-periodic orbits for the Hamiltonian system defined by Eq. (13). These solutions give rise to quasi-periodic motions in $\mathbb{R}^3$ which are not contained in the invariant plane $\{z = 0\}$. Our approach makes use of a technique introduced by Braun in [9], consisting in studying the motion near a global non-isolated minimum of the Hamiltonian. After suitable scalings and canonical transformations the problem is reduced to a perturbation of a 2DOF integrable Hamiltonian with one small frequency, in such a way that Moser's twist theorem can be applied to a suitably defined area-preserving map.

First, let us describe some properties of the potential $V(r,z)$, cf. Eq. (14). It is obvious that $V(r,z) \geq 0$ for any $(r,z) \in \mathbb{R}^+ \times \mathbb{R}$. The computation of the following limits is also

straightforward:

$$\lim_{r\to 0^+} V(r,z) = \infty \text{ if } L_0 \neq 0 \text{ and } 0 \text{ if } L_0 = 0,$$
$$\lim_{r\to 1, z\to 0} V(r,z) = \infty,$$
$$\lim_{r\to \infty} V(r,z) = 0\,.$$

On the other hand $\lim_\infty V(r,z)$ does not exist, which in this case just reflects that $V(r,z)$ has unbounded level sets. The critical points of $V(r,z)$ are given by:

1. If $L_0 > 0$, the potential $V(r,z)$ has a global degenerate minimum given by the closed curve $\{L_0 + I(r,z) = 0\}$. This curve encloses a region which contains the point $(r = 1, z = 0)$, and its diameter tends to ∞ as L_0 tends to 0. Conversely, when L_0 grows the curve shrinks, and it collapses over the point $(1,0)$ in the limit. For $L_0 = 0$ the zero-set of $V(r,z)$ is the z-axis, while for $L_0 < 0$ the potential does not have any local minimum and it is strictly positive.

2. For every $L_0 \in \mathbb{R}$, the potential has a non-degenerate saddle point $(r_M, 0)$ defined by the equation
$$r_M \partial_r I(r_M, 0) - I(r_M, 0) = L_0. \tag{17}$$
Note that for $L_0 > 0$ ($L_0 < 0$), the saddle r_M obtained from Eq. (17) corresponds to the maximum r_M (minimum r_m) of the reduced potential $W(r)$ that we computed in Lemma 4.2. In particular, $r_M > 1$ if $L_0 > 0$, $r_M < 1$ for $L_0 < 0$ and there is no saddle point when $L_0 = 0$ (r_M degenerates to 0). The saddle point is very important because the change of topology of the level sets of $V(r,z)$ exactly happens on the curve of value $V(r_M, 0)$. Recall from Lemma 4.2 that $V(r_M, 0)$ is called the escape energy E_{escape}. In Fig. 4 the potential $V(r,z)$ is plotted for three different values of L_0 to illustrate the three different behaviours depending on the sign of L_0.

When $L_0 > 0$ the Hamiltonian H, cf. Eq. (13), has a global minimum on the curve $\Gamma_{L_0} := \{I(r,z) = -L_0, p_r = 0, p_z = 0\}$. The points in Γ_{L_0} are hence equilibrium positions of the motion, and the level sets of H near Γ_{L_0} are compact submanifolds diffeomorphic to $\mathbb{S}^1 \times \mathbb{S}^2$. The limit energy which guarantees confinement is the escape energy E_{escape}, because it is the value for which all the connected components of $\{V(r,z) = c\}$, $c \geq E_{\text{escape}}$, become unbounded. Hence for values $H_0 < E_{\text{escape}}$ all the motions are bounded because they remain on a compact energy surface, provided that the initial condition is in the bounded component of $H^{-1}([0, E_{\text{escape}}))$.

In the configuration space $\mathbb{R}^3$ (i.e. including the coordinate ϕ), the region of allowed motions is given by $\{V(r,z) \leq H_0\} \times \mathbb{S}^1$. Therefore we can define the *trapping region* as the bounded component of the set
$$\{V(r,z) < E_{\text{escape}}\} \times \mathbb{S}^1\,,$$

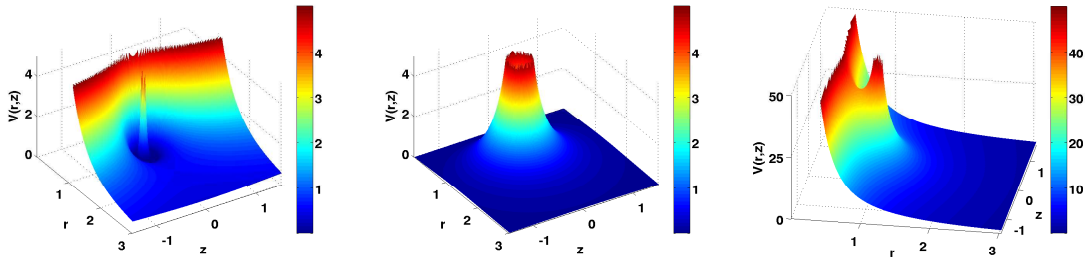

(a) $L_0 = 4$. (b) $L_0 = 0$. (c) $L_0 = -4$.

Figure 4: Graph of the potential $V(r, z)$ for several values of L_0.

which depends on L_0, and is diffeomorphic to $\mathbb{S}^1 \times \mathbb{S}^1 \times (-\varepsilon, \varepsilon)$. This region contains the torus $\{I(r, z) + L_0 = 0\} \times \mathbb{S}^1$. This is similar to the Van Allen inner radiation belt in the Earth magnetosphere, and the possibility of using it to construct a magnetic trap will be discussed in Section 4.4.

Let us observe that when $L_0 \leq 0$ all the connected components of the region $\{V(r, z) \leq H_0\}$ are non-compact for any $H_0 > 0$, and hence all the motions are unbounded (for a proof see Section 4.5), except for some periodic and quasi-periodic trajectories on the invariant plane described in Section 4.2 and possibly a null-measure set outside this plane. For this reason we shall restrict to positive values of L_0. The following theorem shows that the trapping region contains many quasi-periodic motions.

Theorem 4.3. *For any value of $L_0 > 0$ there exist quasi-periodic solutions of the Hamiltonian system defined by Eqs.* (13) *and* (14)*, i.e.*

$$H(r, z, p_r, p_z) = \frac{1}{2}(p_r^2 + p_z^2) + \frac{(L_0 + I(r, z))^2}{2r^2}\,, \tag{18}$$

at a distance ε of Γ_{L_0}.

First, we introduce local coordinates around the degenerate minimum curve $\{I(r, z) + L_0 = 0\}$. To this end, we consider an analytic function $F : U \to \mathbb{S}^1$ which is orthogonal to I, i.e. $\nabla F \cdot \nabla I = 0$ in U. Here the domain $U \subset \mathbb{R}^+ \times \mathbb{R}$ is a tubular neighbourhood of $\{I(r, z) + L_0 = 0\}$. It is clear that one can choose U small enough so that (I, F) diffeomorphically maps U onto $(-L_0 - \delta, -L_0 + \delta) \times \mathbb{S}^1$ and $I^{-1}(c_1) \cong \{c_1\} \times \mathbb{S}^1$, $F^{-1}(c_2) \cong (-L_0 - \delta, -L_0 + \delta) \times \{c_2\}$ for any $c_1 \in (-L_0 - \delta, -L_0 + \delta)$ and $c_2 \in \mathbb{S}^1$. Now let us consider the generating function

$$G(r, z, p_x, p_y) = F(r, z)p_x + I(r, z)p_y,$$

which is defined in $U \times \mathbb{R}^2$. This yields the symplectic transformation

$$\begin{aligned} x &= F(r,z)\,, \\ y &= I(r,z)\,, \\ p_r &= \partial_r F(r,z)p_x + \partial_r I(r,z)p_y\,, \\ p_z &= \partial_z F(r,z)p_x + \partial_z I(r,z)p_y\,, \end{aligned} \tag{19}$$

mapping $U \times \mathbb{R}^2$ onto $(x, y, p_x, p_y) \in \mathbb{S}^1 \times (-L_0 - \delta, -L_0 + \delta) \times \mathbb{R}^2$. In terms of the new coordinates, the Hamiltonian reads as

$$H(x,y,p_x,p_y) = \frac{1}{2}(h_F p_x^2 + h_I p_y^2) + \frac{(L_0+y)^2}{2r^2(x,y)},$$

where $h_F(x,y) := (\nabla F)^2(x,y)$ and $h_I(x,y) := (\nabla I)^2(x,y)$. In these coordinates the curve Γ_{L_0} is given by $\mathbb{S}^1 \times \{-L_0\} \times \{(0,0)\}$. As we discussed previously, there is a region of bounded solutions near the curve Γ_{L_0}, which corresponds to small values of the energy. This region can be studied introducing the scaling

$$\begin{aligned} x &= \varepsilon X\,, \\ y + L_0 &= \varepsilon Y\,, \\ p_x &= \varepsilon p_X\,, \\ p_y &= \varepsilon p_Y\,, \end{aligned}$$

which gives rise to the new Hamiltonian

$$\begin{aligned} H_\varepsilon(X,Y,p_X,p_Y) &:= \varepsilon^{-2} H(\varepsilon X, \varepsilon Y - L_0, \varepsilon p_X, \varepsilon p_Y) \\ &= \frac{1}{2}\left(h_F(\varepsilon X, \varepsilon Y - L_0)p_X^2 + h_I(\varepsilon X, \varepsilon Y - L_0)p_Y^2 \right) + \frac{Y^2}{2r^2(\varepsilon X, \varepsilon Y - L_0)} \\ &= \frac{1}{2}a(\varepsilon X)p_X^2 + \frac{1}{2}b(\varepsilon X)p_Y^2 + \frac{1}{2}c(\varepsilon X)Y^2 + \varepsilon g(X,Y,p_X,p_Y;\varepsilon). \end{aligned}$$

To obtain the last expression we have expanded the functions $h_F(x,y)$, $h_I(x,y)$ and $r^{-2}(x,y)$ around $y = -L_0$, i.e. $h_F(x,y) = a(x) + O(y+L_0)$, $h_I(x,y) = b(x) + O(y+L_0)$ and $r^{-2}(x,y) = c(x) + O(y+L_0)$. In the scaled variables the remaining terms are of the form $O(y+L_0) = \varepsilon O(Y;\varepsilon)$, and putting all together we get the function $\varepsilon g(X,Y,p_x,p_Y;\varepsilon)$. Let us observe that the functions $a, b, c : \mathbb{S}^1 \to \mathbb{R}$ do not vanish because $(\nabla I)^2$, $(\nabla F)^2$ and r^{-2} are never zero on the curve $\{I(r,z) + L_0 = 0\}$.

Neglecting the perturbative term εg, the Hamiltonian H_ε is of harmonic oscillator type in the variables (Y, p_Y). This suggests to introduce the following generating function

$$S(X,Y,p_{\tilde{x}},p_{\tilde{y}}) = v(\varepsilon X)^{1/4} Y p_{\tilde{y}} + X p_{\tilde{x}}, \qquad v(\varepsilon X) := \frac{c(\varepsilon X)}{b(\varepsilon X)}\,,$$

in order to write this harmonic oscillator in a canonical form. The resulting symplectic transformation, which is given by

$$\begin{aligned} X &= \tilde{x}\,, \\ Y &= v(\varepsilon\tilde{x})^{-1/4}\tilde{y}\,, \\ p_X &= p_{\tilde{x}} + \frac{\varepsilon}{4}\frac{v'(\varepsilon\tilde{x})}{v(\varepsilon\tilde{x})}\tilde{y}p_{\tilde{y}}\,, \\ p_Y &= v(\varepsilon\tilde{x})^{1/4}p_{\tilde{y}}\,, \end{aligned}$$

allows us to write the Hamiltonian in the form

$$\tilde{H}_\varepsilon(\tilde{x},\tilde{y},p_{\tilde{x}},p_{\tilde{y}}) = \frac{1}{2}a(\varepsilon\tilde{x})p_{\tilde{x}}^2 + \frac{1}{2}\tilde{b}(\varepsilon\tilde{x})\left(p_{\tilde{y}}^2+\tilde{y}^2\right) + \varepsilon\tilde{g}(\tilde{x},\tilde{y},p_{\tilde{x}},p_{\tilde{y}};\varepsilon),$$

where $\tilde{b}(\varepsilon\tilde{x}) := \sqrt{b(\varepsilon\tilde{x})c(\varepsilon\tilde{x})}$.

If we introduce the "action" variable $R_1 = \frac{1}{2}(p_{\tilde{y}}^2+\tilde{y}^2)$ associated to the harmonic oscillator we end up with the Hamiltonian

$$\tilde{H}_\varepsilon(\tilde{x},\theta_1,p_{\tilde{x}},R_1) = \frac{1}{2}a(\varepsilon\tilde{x})p_{\tilde{x}}^2 + \tilde{b}(\varepsilon\tilde{x})R_1 + \varepsilon\tilde{g}(\tilde{x},\theta_1,p_{\tilde{x}},R_1;\varepsilon).$$

In order to apply Moser's twist theorem it is convenient to change the parametrisation of time. The way of doing this, preserving the Hamiltonian character, is to define a new Hamiltonian function

$$F_{\varepsilon,h}(\tilde{x},\theta_1,p_{\tilde{x}},R_1) := \frac{\tilde{H}_\varepsilon(\tilde{x},\theta_1,p_{\tilde{x}},R_1)-h}{\tilde{b}(\varepsilon\tilde{x})}\,.$$

It is clear that the Hamiltonian vector field associated to $F_{\varepsilon,h}$ on the level $\{F_{\varepsilon,h}=0\}$ is proportional to that of $\tilde{H}_\varepsilon$ on the level $\{\tilde{H}_\varepsilon = h\}$, the proportionality factor being $\tilde{b}(\varepsilon\tilde{x})^{-1}$. So we can study the solutions of the Hamiltonian $\tilde{H}_\varepsilon$ by fixing a constant h and studying the Hamiltonian

$$F_{\varepsilon,h} = R_1 + \frac{a(\varepsilon\tilde{x})}{2\tilde{b}(\varepsilon\tilde{x})}p_{\tilde{x}}^2 - \frac{h}{\tilde{b}(\varepsilon\tilde{x})} + \varepsilon\tilde{g}_1(\tilde{x},\theta_1,p_{\tilde{x}},R_1;\varepsilon)\,,$$

where $\tilde{g}_1 := \tilde{g}/\tilde{b}$. Neglecting the perturbative term $\tilde{g}_1$, the Hamiltonian $F_{\varepsilon,h}$ is integrable, and hence it is relevant to study the solutions of the 1DOF Hamiltonian system

$$F^0_{\varepsilon,h} := \frac{a(\varepsilon\tilde{x})}{2\tilde{b}(\varepsilon\tilde{x})}p_{\tilde{x}}^2 - \frac{h}{\tilde{b}(\varepsilon\tilde{x})} \tag{20}$$

on the cylinder $(\tilde{x},p_{\tilde{x}}) \in \mathbb{S}^1\times\mathbb{R}$.

Lemma 4.4. *The function $\tilde{b}(\varepsilon\tilde{x}) : \mathbb{S}^1 \to \mathbb{R}$ is not identically constant for any value of $L_0 > 0$, and hence it reaches a maximum and a minimum value on $\mathbb{S}^1$.*

Proof. By definition we have that $\tilde{b}(\varepsilon\tilde{x})$ is written in the original coordinates (r, z) as

$$\tilde{b} = \frac{|\nabla I(r,z)|}{r}\Big|_{\{I(r,z)+L_0=0\}} = |B_{\mathcal{C}}|\Big|_{\{I(r,z)+L_0=0\}},$$

where Eq. (9) has been used to get the last equality. Therefore, $\tilde{b}$ turns out to be the Euclidean norm of the magnetic field $B_{\mathcal{C}}$ on the magnetic line $\{I(r,z)+L_0=0\}$. To prove that $|B_{\mathcal{C}}|$ is not constant on any magnetic line, it is enough to consider the intersection of $\{I(r,z)+L_0=0\}$ with the r-axis, which defines two values of r for each $L_0 > 0$, denoted in Lemma 4.2 by $r_{m_1} < r_{m_2}$. It is clear from Fig. 3(b) that $|\partial_r I(r_{m_1}, 0)| > |\partial_r I(r_{m_2}, 0)|$, which implies that $|B_{\mathcal{C}}(r_{m_1}, 0)| > |B_{\mathcal{C}}(r_{m_2}, 0)|$, and hence $|B_{\mathcal{C}}|$ cannot be constant on the line $\{I(r,z) = L_0\}$, thus proving the stated result. □

A straightforward computation shows that the critical points of the Hamiltonian $F^0_{\varepsilon,h}$ on the cylinder $(\tilde{x}, p_{\tilde{x}})$ are given by $(\tilde{x}, 0)$, with $\tilde{x}$ satisfying the equation $\tilde{b}'(\varepsilon\tilde{x}) = 0$. On account of Lemma 4.4, there are, at least, two solutions to this equation: the one which corresponds to the global minimum $\tilde{x}_m$ of $\tilde{b}(\varepsilon\tilde{x})$ on $\mathbb{S}^1$, and the one corresponding to the global maximum $\tilde{x}_M$ of $\tilde{b}(\varepsilon\tilde{x})$.

It is easy to check that for $h > 0$ the point $(\tilde{x}_m, 0)$ is a local minimum of $F^0_{\varepsilon,h}$, while the point $(\tilde{x}_M, 0)$ is a saddle point, and conversely if $h < 0$. Let us fix, without loss of generality, a positive value for the constant h. From this analysis we conclude that the phase portrait of the Hamiltonian vector field defined by $F^0_{\varepsilon,h}$ has a critical point of centre type at $(\tilde{x}_m, 0)$, and the boundary of the corresponding periodic region is a saddle loop formed by the stable and unstable components of the critical point $(\tilde{x}_M, 0)$.

This allows us to define an action variable R_2 associated to the coordinates $(\tilde{x}, p_{\tilde{x}})$ in a periodic region of $F^0_{\varepsilon,h}$, which yields the following expression for the Hamiltonian $F_{\varepsilon,h}$

$$F_{\varepsilon,h} = R_1 + f(\varepsilon R_2) + \varepsilon\tilde{g}_2(\theta_1, \theta_2, R_1, \varepsilon R_2; \varepsilon),$$

which verifies the condition

$$f''(\varepsilon R_2) \neq 0. \tag{21}$$

This is because the frequency of the periodic solutions in the centre region of $F^0_{\varepsilon,h}$ is given by $\varepsilon f'(\varepsilon R_2)$. To see that this function is not a constant just note that the period tends to infinity when approaching the boundary of the centre domain (the saddle loop).

The corresponding equations of motion are

$$\begin{aligned}
\dot{\theta}_1 &= 1 + \varepsilon\partial_{R_1}\tilde{g}_2, \\
\dot{\theta}_2 &= \varepsilon f'(\varepsilon R_2) + \varepsilon^2\partial_{\varepsilon R_2}\tilde{g}_2, \\
\dot{R}_1 &= \varepsilon\partial_{\theta_1}\tilde{g}_2, \\
\dot{R}_2 &= \varepsilon\partial_{\theta_2}\tilde{g}_2.
\end{aligned}$$

Now we consider the Poincaré section defined by $\{\theta_1 = 0\}$ on the submanifold $\{F_{\varepsilon,h} = 0\}$. First, we eliminate the variable R_1 from equation $F_{\varepsilon,h}(\theta_2, \theta_1, R_1, \varepsilon R_2; \varepsilon) = 0$ and, using θ_1 as independent variable instead of t, the equations of motion give rise to

$$\frac{d\theta_2}{d\theta_1} = \varepsilon f'(\varepsilon R_2) + \varepsilon^2 A_1(\theta_2, \theta_1, \varepsilon R_2; \varepsilon)\,,$$
$$\frac{dR_2}{d\theta_1} = \varepsilon A_2(\theta_2, \theta_1, \varepsilon R_2; \varepsilon)\,,$$

so we compute the return map by solving this non-autonomous system of differential equations for θ_2 and R_2. A formal integration of these equations from $\theta_1 = 0$ to $\theta_1 = 2\pi$ defines the return map on the chosen Poincaré section. This is a symplectic map which in coordinates $\alpha := \theta_2$ and $J := \varepsilon R_2$ reads as

$$M_\varepsilon : \begin{pmatrix} \alpha \\ J \end{pmatrix} \longmapsto \begin{pmatrix} \alpha + \varepsilon f'(J) + O(\varepsilon^2) \\ J + O(\varepsilon^2) \end{pmatrix}.$$

This map is a perturbation of order ε^2 of a twist map with small rotation number of order ε. Since the non-degeneracy (or twist) condition $f''(J) \neq 0$ is fulfilled (recall the argument following Eq. (21)), this is enough to apply Moser's twist theorem to M_ε because the perturbation is small compared to the twist $\varepsilon f'(J)$, cf. [9, 36]. Therefore, taking into account all the previous discussion, we finally conclude the existence of quasi-periodic solutions provided that ε is sufficiently small, as we desired to prove. In fact, from the previous analysis it is standard (using Poincaré-Birkhoff fixed point theorem for perturbations of twist maps) to conclude the following.

Corollary 4.5. *For any value of $L_0 > 0$ there exist periodic solutions of the Hamiltonian system defined by Eq.* (18) *at a distance ε of Γ_{L_0}.*

4.4 A technical application: magnetic traps

As discussed at the beginning of Section 4.3, the saddle point given by Eq. (17) defines a trapping region for the motion of a charged particle in the magnetic field created by a loop wire. This domain depends on the value of L_0, and it is given by a tubular neighbourhood of the torus $\{I(r,z) + L_0 = 0\} \times \mathbb{S}^1 \subset \mathbb{R}^3$. The limit energy for which we have confinement is E_{escape}. Let us now show how this escape energy can be modified by changing the current intensity $J_{\mathcal{C}}$, so that some scattering trajectories can become bounded.

The use of a circular wire to construct magnetic traps has a long tradition. In the typical constructions, another field (electric or magnetic) is superposed to the magnetic field of the wire to trap neutral atoms [34, 44]. The interaction is by means of the magnetic moment of the atom, and the trapping region is a narrow cylinder along the z-axis. Similar trapping regions have been obtained for charged particles with magnetic moment, where a magnetic bottle can

be constructed near the centre of the circular wire, cf. [10, Section VI-D], [21]. The magnetic trap that we shall describe below is completely different to these ones, and as far as we know, it is new. It is based on the trapping region that we proved to exist in Section 4.3, and the magnetic bottle that we create this way is a toroidal annulus around the wire.

All along this section we assume that $L_0 > 0$. Let us consider a charged particle with initial condition $(r_0, z_0, \phi_0, \dot{r}_0, \dot{z}_0, \dot{\phi}_0)$ moving under the action of $B_{\mathcal{C}}$. The current intensity is relevant for our analysis, so we shall write it explicitly in all the formulae. Then, the particle motion can be described as a solution of the Hamiltonian system

$$H(r, z, p_r, p_z) = \frac{1}{2}(p_r^2 + p_z^2) + V(r, z), \qquad V(r, z) = \frac{(L_0 + J_{\mathcal{C}} I(r, z))^2}{2r^2}\,, \tag{22}$$

where $L_0 = r_0^2\dot{\phi}_0 - J_{\mathcal{C}} I(r_0, z_0)$ and H_0 is determined by the initial condition.

Assume that at certain time t_1 the position of the charge is $(r_1, \phi_1, z_1) \in \mathcal{T}$, and the velocity is $(\dot{r}_1, \dot{\phi}_1, \dot{z}_1)$. The domain $\mathcal{T}$ is the trapping region defined in Section 4.3, that is

$$\mathcal{T} := \text{bounded component of } \{(r, z) \in \mathbb{R}^+ \times \mathbb{R} : V(r, z) < E_{\text{escape}}\} \times \mathbb{S}^1\,.$$

The charge reaches this position if we send the particle with energy $H_0 > E_{\text{escape}}$ in the direction of the trapping region. However, note that the charge is not trapped and eventually escapes to infinity, possibly after some transient of time in the region of confinement. Now the idea is to change the current intensity in order to modify the escape energy, thus getting the desired trap. For the sake of simplicity we will assume a sudden and small change of intensity, neglecting the creation of an electromagnetic field in the process and radiative phenomena.

If at $t_1 > 0$ we change the current intensity from $J_{\mathcal{C}}$ to $\tilde{J}_{\mathcal{C}}$, we get that the constant L_0 changes as

$$\tilde{L}_0 = r_1^2\dot{\phi}_1 - \tilde{J}_{\mathcal{C}} I(r_1, z_1) = L_0 + (J_{\mathcal{C}} - \tilde{J}_{\mathcal{C}}) I(r_1, z_1)\,, \tag{23}$$

and the new Hamiltonian turns out to be

$$\tilde{H}(r, z, p_r, p_z) = \frac{1}{2}(p_r^2 + p_z^2) + \frac{(\tilde{L}_0 + \tilde{J}_{\mathcal{C}} I(r, z))^2}{2r^2}\,.$$

Let us observe that the energy of the particle is the same, since (using Eq. (23))

$$\tilde{H}_0 - H_0 = \frac{(\tilde{L}_0 + \tilde{J}_{\mathcal{C}} I(r_1, z_1))^2 - (L_0 + J_{\mathcal{C}} I(r_1, z_1))^2}{2r_1^2} = 0.$$

Therefore, if we prove that E_{escape} is increasing with $\tilde{J}_{\mathcal{C}}$ we can choose $\tilde{J}_{\mathcal{C}} > J_{\mathcal{C}}$ so that $H_0 < \tilde{E}_{\text{escape}}$, thus trapping the particle.

The simplest situation is when $J_{\mathcal{C}} = 0$. In this case there is no magnetic field, the motion is free, with $L_0 = r_1^2\dot{\phi}_1$ and $E_{\text{escape}} = 0$ so $\mathcal{T} = \emptyset$. When intensity current $\tilde{J}_{\mathcal{C}} > 0$ is added we immediately obtain that $\tilde{E}_{\text{escape}} > 0$, and hence we get a trap for particles with energy $H_0 < \tilde{E}_{\text{escape}}$ provided that (r_1, z_1) belongs to the bounded component of $\{\tilde{V}(r, z) < H_0\}$. As

the change of intensity is small, the current $\tilde{J}_{\mathcal{C}}$ is close to zero, and hence the new trapping region is very narrow because the saddle point $(\tilde{r}_M, 0)$ is near the singularity $(1, 0)$. Accordingly, it is more advantageous to consider that $J_{\mathcal{C}} > 0$ before the change of intensity, which allows us to obtain bigger trapping regions.

Under this assumption, let us show that an increment of the current intensity implies that $\tilde{E}_{\text{escape}} > E_{\text{escape}}$. It is convenient to define the set

$$\mathcal{T}_I := \{(r, z) \in \mathbb{R}^+ \times \mathbb{R} : I(r, z) < I(r_M, 0)\} \times \mathbb{S}^1 \,,$$

where $(r_M, 0)$ is the position of the saddle of the potential $V(r, z)$. Using the properties of the functions $I(r, z)$ and $V(r, z)$ it is not difficult to check that $\mathcal{T} \subset \mathcal{T}_I$, and hence the point where the current intensity is changed verifies $(r_1, \phi_1, z_1) \in \mathcal{T}_I$. The key observation to obtain a magnetic trap is the following:

Proposition 4.6. *Given $J_{\mathcal{C}} > 0$, let us assume that the Hamiltonian* (22) *has a solution that at certain time $t_1 > 0$ satisfies $(r_1, \phi_1, z_1) \in \mathcal{T}$ with energy $H_0 > E_{\text{escape}}$. Then, if we increase the current intensity up to $\tilde{J}_{\mathcal{C}} > J_{\mathcal{C}}$, we obtain that $\tilde{E}_{\text{escape}} > E_{\text{escape}}$ and $(r_1, \phi_1, z_1) \in \tilde{\mathcal{T}}$, where*

$$\tilde{\mathcal{T}} := \textit{bounded component of } \{(r, z) \in \mathbb{R}^+ \times \mathbb{R} : \tilde{V}(r, z) < \tilde{E}_{\text{escape}}\} \times \mathbb{S}^1 \,.$$

Proof. First, let us observe that the position of the saddle point of $\tilde{V}(r, z)$ is $(\tilde{r}_M, 0)$ satisfying Eq. (17), which now reads as

$$\tilde{J}_{\mathcal{C}} \tilde{r}_M \partial_r I(\tilde{r}_M, 0) - \tilde{J}_{\mathcal{C}} I(\tilde{r}_M, 0) = \tilde{L}_0 \,,$$

and introducing this expression into $\tilde{V}(\tilde{r}_M, 0)$ we obtain that the new escape energy is

$$\tilde{E}_{\text{escape}} = \frac{\tilde{J}_{\mathcal{C}}^2}{2} \Big[\partial_r I(\tilde{r}_M, 0)\Big]^2 .$$

We divide the proof in two cases:

Case 1: Assume that $L_0 + J_{\mathcal{C}} I(r_1, z_1) \leq 0$. It is easy to check, by computing its derivative, that the quantity

$$\frac{\tilde{L}_0}{\tilde{J}_{\mathcal{C}}} = \tilde{r}_M \partial_r I(\tilde{r}_M, 0) - I(\tilde{r}_M, 0) = \frac{L_0 + (J_{\mathcal{C}} - \tilde{J}_{\mathcal{C}}) I(r_1, z_1)}{\tilde{J}_{\mathcal{C}}} \tag{24}$$

is increasing with $\tilde{J}_{\mathcal{C}}$ provided that $L_0 + J_{\mathcal{C}} I(r_1, z_1) < 0$, therefore if $\tilde{J}_{\mathcal{C}} > J_{\mathcal{C}}$, the radius becomes $\tilde{r}_M < r_M$ (cf. Fig. 3(a)). On account of Fig. 3(b) we get that $\partial_r I(\tilde{r}_M, 0) > \partial_r I(r_M, 0)$, thus concluding that $\tilde{E}_{\text{escape}} > E_{\text{escape}}$. When $L_0 + J_{\mathcal{C}} I(r_1, z_1) = 0$, it follows that $\tilde{r}_M = r_M$ and $\tilde{E}_{\text{escape}} = \frac{\tilde{J}_{\mathcal{C}}}{J_{\mathcal{C}}} E_{\text{escape}} > E_{\text{escape}}$. Roughly speaking, the trapping region becomes deeper (in the sense that allows higher energies) than the initial one but, on the contrary, it is narrower (because $\tilde{r}_M \leq r_M$).

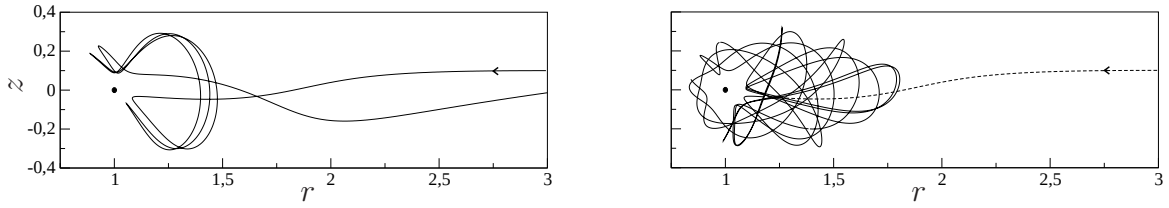

(a) Particle of energy $H_0 = 0.7$ and initial conditions $r_0 = 3$, $z_0 = 0.1$, $\dot{r}_0 = -0.678502$, $\dot{z}_0 = 0$ and $L_0 = 4$, under a current $J_{\mathcal{C}} = 1$.

(b) Under the same conditions of (a), the intensity is increased to $\tilde{J}_{\mathcal{C}} = 1.05$ when $J_{\mathcal{C}} I(r_1, z_1) + L_0 = 0$.

Figure 5: Numerical verification of the use of the circular wire as a magnetic trap. (a) The particle enters the scattering region created by the circular wire and it is scattered after a short transient time because $H_0 > E_{\text{escape}} = 0.635247$. (b) Since $\tilde{E}_{\text{escape}} = 0.700371 > H_0 = 0.7$, the particle is trapped indefinitely in a torus-like neighbourhood of the wire (the dashed line shows the trajectory under $J_{\mathcal{C}} = 1$, and the solid line shows the trajectory after the increment of current intensity to $\tilde{J}_{\mathcal{C}} = 1.05$). Note: As a reference, the intersection of the wire with the (r, z) half-plane is plotted in both pictures.

Case 2: Assume that $L_0 + J_{\mathcal{C}} I(r_1, z_1) > 0$. In this case the quantity defined by Eq. (24) is decreasing with $\tilde{J}_{\mathcal{C}}$, and hence $\tilde{r}_M > r_M$ and $I(\tilde{r}_M, 0) > I(r_M, 0)$. A straightforward computation shows that

$$\frac{d\tilde{E}_{\text{escape}}}{d\tilde{J}_{\mathcal{C}}} = \frac{\tilde{J}_{\mathcal{C}} \partial_r I(\tilde{r}_M, 0)}{\tilde{r}_M} \Big(I(\tilde{r}_M, 0) - I(r_1, z_1) \Big),$$

which is positive because $I(r_1, z_1) < I(r_M, 0)$ (by assumption $(r_1, \phi_1, z_1) \in \mathcal{T} \subset \mathcal{T}_I$) and $\partial_r I(\tilde{r}_M, 0) > 0$ for $\tilde{r}_M > 1$ (see Fig. 3(b)). Therefore $\tilde{E}_{\text{escape}} > E_{\text{escape}}$ if $\tilde{J}_{\mathcal{C}} > J_{\mathcal{C}}$, as we desired to prove. In this case the trapping region is not only deeper but it becomes wider since $\tilde{r}_M > r_M$.

Finally, it is clear that $V(r_1, z_1) = \tilde{V}(r_1, z_1)$ so $(r_1, \phi_1, z_1) \in \tilde{\mathcal{T}}$. □

In physical terms we have that by increasing the current intensity (and hence the field strength $|B_{\mathcal{C}}|$) we can trap charges which are in the region $\mathcal{T}$ and which otherwise would escape to infinity (see Fig. 5 for a numerical example of this phenomenon). The reason is that the escape energy also increases, and so the level line $\{\tilde{V}(r, z) = H_0\}$, which was previously open, now becomes closed.

Finally, to be sure that we obtain an optimal confinement (in the sense that $\tilde{E}_{\text{escape}}$ is maximum and that we trap as many particles as possible), we should change the current intensity

when (r_1, z_1) is such that $\tilde{J}_{\mathcal{C}} I(r_1, z_1) + \tilde{L}_0$ is near 0, that is, when the particles are near the minimum of the potential $\tilde{V}(r, z)$. This is consistent with the case 1 where $J_{\mathcal{C}} I(r_1, z_1) + L_0 \leq 0$, because it easily follows that $\{\tilde{J}_{\mathcal{C}} I(r_1, z_1) + \tilde{L}_0 = 0\} \subset \{J_{\mathcal{C}} I(r_1, z_1) + L_0 \leq 0\}$.

This method becomes quite effective when we have a stream of charges which is directed over the ring wire. In this case a high fraction of particles will be trapped after increasing the intensity, with more chance of being confined when the energy $H_0 \simeq E_{\text{escape}}$. Let us observe that charges are trapped for all time $t > t_1$, and hence this phenomenon goes beyond the adiabatic approximation. We also want to remark that this trapping region is not associated to a minimum of $|B_{\mathcal{C}}|$, which is the standard procedure in the literature of magnetic traps [10, 34, 44], but to a magnetic line. Accordingly, the confinement region is not a cylinder around certain point but a torus-like domain.

4.5 Existence of scattering trajectories

We have proved in Section 4.2, by reducing the problem to a 1DOF Hamiltonian system, that there are solutions which escape to infinity on the invariant plane $\{z = 0\}$. On the other hand, the level sets of the potential $V(r, z)$, cf. Section 4.3, suggest that there are many unbounded solutions which are not contained in the invariant plane. A first observation is that the solutions to Eqs. (13) and (14) are defined for all t, so they cannot escape to infinity in finite time. This is easily proved using the conservation of energy and that $|\nabla V(r, z)|$ is bounded for each trajectory.

The goal of this section is to prove the existence of scattering motions away from the invariant plane for $L_0 > 0$. The case $L_0 \leq 0$ is elementary and will be discussed at the end of this section. The main idea consists in studying the equation for the radial coordinate $\rho := \sqrt{r^2 + z^2}$ in the (r, z) half-plane. Then, using some inequalities, we can show that the solution $\rho(t)$ tends to infinity when $t \to \infty$ for suitable initial conditions.

Let us consider the Newton-Lorentz equations associated to the effective potential $V(r, z)$, cf. Eq. (14). The following inequality is standard:

$$\ddot{\rho} \geq \frac{r\ddot{r} + z\ddot{z}}{\rho} = -\frac{r\partial_r V(r, z) + z\partial_z V(r, z)}{\rho}\,,$$

and using the definition of $V(r, z)$, a straightforward computation yields the expression

$$\ddot{\rho} \geq -\frac{(L_0 + I(r, z))(r\partial_r I(r, z) + z\partial_z I(r, z) - L_0 - I(r, z))}{r^2(r^2 + z^2)^{1/2}}\,.$$

As stated in Lemma 4.1, if $L_0 > 0$ the set $\{L_0 + I(r, z) = 0\}$ is a closed curve bounding a region which contains the point $(r = 1, z = 0)$. It is clear that $L_0 + I(r, z) > 0$ if $\rho > C(L_0)$ for some large enough constant which depends on L_0. Therefore, when $\rho > C(L_0)$ the sign of the right hand side of the above inequality is determined by the sign of $r\partial_r I(r, z) + z\partial_z I(r, z) - L_0 - I(r, z)$.

Lemma 4.7. *For any $L_0 > 0$, there exists a positive constant $Q(L_0)$ for which the inequality $r\partial_r I(r,z) + z\partial_z I(r,z) - L_0 - I(r,z) < 0$ holds if $\rho = \sqrt{r^2+z^2} > Q(L_0)$.*

Proof. It is enough to show that $\lim_{\rho\to\infty}(r\partial_r I(r,z) + z\partial_z I(r,z) - I(r,z)) = 0$, because in that case you can choose a large enough constant $Q(L_0)$ for which $r\partial_r I(r,z)+z\partial_z I(r,z)-I(r,z) < L_0$ if $\rho > Q(L_0)$. As $\lim_{\rho\to\infty} k^2 = 0$, cf. Eq. (11), the definition (10) of $I(r,z)$ implies, doing a Taylor expansion around $k=0$, the following equation:

$$I(r,z) = \frac{-\pi r^2}{((1+r)^2+z^2)^{3/2}} + \varepsilon(r,z)\,,$$

where $\lim_{\rho\to\infty} \frac{((1+r)^2+z^2)^{3/2}\varepsilon(r,z)}{r^2} = 0$. Taking derivatives with respect to r and z we obtain, after some computations, the formula

$$r\partial_r I(r,z) + z\partial_z I(r,z) - I(r,z) = \frac{-\pi r^2(1-2r^2-r-2z^2)}{((1+r)^2+z^2)^{5/2}} + \tilde{\varepsilon}(r,z)\,,$$

whose limit as $\rho\to\infty$ is zero, thus proving the desired result. □

Taking into account Lemma 4.7 and the previous discussion we conclude that

$$\ddot{\rho} > 0$$

provided that $\rho > \max\{C(L_0), Q(L_0)\} := \kappa(L_0)$. If we have an initial condition for which $\rho_0 > \kappa(L_0)$ and $\dot{\rho}_0 > 0$ it is easy to check that the solution $\rho(t)$ is increasing with t and in fact $\lim_{t\to\infty}\rho(t) = \infty$, otherwise there would be a change of concavity in the graph $(t,\rho(t))$ contradicting the fact that $\ddot{\rho} > 0$ if $\rho > \kappa(L_0)$. This proves the existence of scattering solutions.

This result shows that (at least) one of the coordinates either r or z is unbounded when $t\to\infty$. In fact we can show that there are solutions which escape to infinity in the r coordinate. Indeed, let us consider the Newton-Lorentz equation for the r variable, cf. Eqs. (13) and (14), which is

$$\ddot{r} = \frac{(L_0 + I(r,z))(L_0 - (r\partial_r I(r,z) - I(r,z)))}{r^3}\,,$$

with initial conditions r_0 and $\dot{r}_0 > 0$. The same argument as in Lemma 4.7 shows that $\lim_{r\to\infty}(r\partial_r I(r,z) - I(r,z)) = 0$, and hence proceeding as in the previous discussion we can prove that $\ddot{r}(t) > 0$ for all $t \geq 0$, provided that $r_0 > \kappa(L_0)$ for some constant κ which depends on L_0 (this does not depend on the sign of L_0). Accordingly there are solutions for which $\lim_{t\to\infty} r(t) = \infty$. This is in strong contrast with the motion in the magnetic field of a rectilinear wire, cf. Section 3, where all the trajectories of the charge are periodic in the r coordinate.

This escape in the r coordinate is less general than the scattering solutions proved to exist when working with the variable ρ. For example, there are unbounded solutions with $r_0 < 1$ and $\dot{r}_0 \leq 0$, provided that z_0 and $\dot{z}_0$ are large enough to make $\rho_0 > \kappa(L_0)$ and $\dot{\rho}_0 > 0$. Therefore

we can guarantee escape in all possible directions. Let us observe that the relevant parameter for these arguments is not the energy H_0 but the values of ρ_0 and $\dot{\rho}_0$. In particular, the energy is very small for an unbounded solution with large r_0 and small $\dot{r}_0 > 0$, $\dot{z}_0 > 0$, but this is not contradictory because, as explained in Section 4.3, the potential $V(r, z)$ has level curves of small values which are open.

When $L_0 \leq 0$ it is not difficult to prove that almost all the solutions with $z_0^2 + \dot{z}_0^2 \neq 0$ escape to infinity (the case $z_0 = \dot{z}_0 = 0$ corresponds to trajectories which are contained in the invariant plane $\{z = 0\}$, see Section 4.2 for a detailed analysis). Indeed, the Newton-Lorentz equation for the z coordinate, cf. Eqs. (13) and (14), reads as

$$\ddot{z} = -\frac{(L_0 + I(r, z))\partial_z I(r, z)}{r^2}\,.$$

The sign of this equation can be controlled because, on the one hand $-r^{-2}(L_0+I(r, z)) > 0$ and on the other hand $\partial_z I(r, z)$ is proportional to the radial component of the magnetic field $B_{\mathcal{C}}$, cf. Eq. (9), and hence the geometry of the magnetic lines implies that $\partial_z I(r, z) > 0$ if $z > 0$ and $\partial_z I(r, z) < 0$ if $z < 0$. Therefore, when $z_0 > 0$ and $\dot{z}_0 \geq 0$ we have that $\ddot{z}(t) > 0$, which readily implies that $\lim_{t\to\infty} z(t) = \infty$. Analogously, when $z_0 < 0$ and $\dot{z}_0 \leq 0$ we have that $\ddot{z}(t) < 0$, thus yielding that $\lim_{t\to\infty} z(t) = -\infty$. Otherwise, since the invariant plane is unstable (see the discussion at the end of Section 4.2) all the solutions cross the plane $\{z = 0\}$ changing their concavity and hence they escape in the positive or negative direction of the z-axis depending on the sign of $\dot{z}_0$, with the exception of the solutions which belong to the stable component associated to the invariant plane. These exceptional solutions, which define a null-measure set in the $(z_0, \dot{z}_0)$ plane, verify that $\lim_{t\to\infty} z(t) = 0$, so we cannot conclude whether the corresponding trajectories are bounded or not just studying the Newton-Lorentz equation for the z coordinate.

5 Motion in the magnetic field of a coupled system

In this section we study the motion of a charge in the magnetic field created by a circular wire centred at the z-axis, carrying a current of intensity $J_{\mathcal{C}} > 0$ in the direction of the vector field ∂_ϕ, and an infinite rectilinear filament $\mathcal{R}$ with current intensity $J_{\mathcal{R}} > 0$. We shall restrict ourselves to the case in which the circular wire $\mathcal{C}$ lies on the plane $\{z = 0\}$ and $\mathcal{R}$ is defined by a current flowing in the positive direction of the z-axis, in order that the axial symmetry be preserved. In what follows we shall denote this system by $\mathcal{C} + \mathcal{R}$.

As far as we know, there are no rigorous results in the literature concerning this configuration, which turns out to be much more difficult to analyse (global aspects specially) than the single loop wire studied in Section 4. Specifically, we shall be able to prove the existence of quasi-periodic trajectories only when $J_{\mathcal{R}}/J_{\mathcal{C}} \ll 1$. It remains open to provide an analytical study of the case in which $J_{\mathcal{C}}$ and $J_{\mathcal{R}}$ are comparable, which is numerically analysed in Section 6. Finally, we will also prove that, independently of the values of $J_{\mathcal{R}}$ and $J_{\mathcal{C}}$, there are

not scattering solutions for which the quotient $|z(t)|/r(t)$ is bounded, and therefore the escape in the z coordinate is dominant over the escape in the r direction, as in the case of the single rectilinear wire (where $r(t)$ is in fact periodic).

We call $B_{\mathcal{C}+\mathcal{R}}$ the magnetic field created by this system, which is given by

$$B_{\mathcal{C}+\mathcal{R}} = \frac{J_{\mathcal{C}}\partial_z I(r,z)}{r}\,\partial_r + \frac{2J_{\mathcal{R}}}{r^2}\partial_\phi - \frac{J_{\mathcal{C}}\partial_r I(r,z)}{r}\,\partial_z\,,$$

where $I(r,z)$ is defined in Eq. (10). Observe that $B_{\mathcal{C}+\mathcal{R}}$ is analytic in $\mathbb{R}^3\backslash(\mathcal{C}\cup\mathcal{R})$ and that $I(r,z)$ is a first integral of this vector field, thus implying that all the magnetic lines of $B_{\mathcal{C}+\mathcal{R}}$ lie on magnetic surfaces which are revolution tori, cf. Lemma 4.1. Moreover, it is not difficult to check, cf. [17], that the integral curves of this field are periodic or quasi-periodic depending on the magnetic surface (in contrast with those of $B_{\mathcal{C}}$ that are all periodic).

The Newton-Lorentz equations of motion of a unit-mass, unit-charge particle subjected to $B_{\mathcal{C}+\mathcal{R}}$ read as

$$\ddot{r} - r\dot{\phi}^2 = -J_{\mathcal{C}}\dot{\phi}\partial_r I(r,z) - \frac{2J_{\mathcal{R}}\dot{z}}{r}\,, \tag{25}$$

$$r^2\ddot{\phi} + 2r\dot{r}\dot{\phi} = J_{\mathcal{C}}\dot{z}\partial_z I(r,z) + J_{\mathcal{C}}\dot{r}\partial_r I(r,z)\,, \tag{26}$$

$$\ddot{z} = -J_{\mathcal{C}}\dot{\phi}\partial_z I(r,z) + \frac{2J_{\mathcal{R}}\dot{r}}{r}\,. \tag{27}$$

This system of equations has two first integrals: the kinetic energy $E := \frac{1}{2}(\dot{r}^2 + r^2\dot{\phi}^2 + \dot{z}^2)$, and the generalized angular momentum $L := r^2\dot{\phi} - J_{\mathcal{C}}I(r,z)$. These conserved quantities allow us to reduce the equations of motion to a 2DOF Hamiltonian system on the half-plane $(r,z)\in\mathbb{R}^+\times\mathbb{R}$, given by:

$$H_{\mathcal{C}+\mathcal{R}}(r,z,p_r,p_z) := \frac{1}{2}\Big(p_r - \frac{2J_{\mathcal{R}}z}{r}\Big)^2 + \frac{1}{2}p_z^2 + V(r,z)\,, \tag{28}$$

with

$$V(r,z) := \frac{(L_0 + J_{\mathcal{C}}I(r,z))^2}{2r^2}\,. \tag{29}$$

Note that this Hamiltonian is not written in natural form due to the new term z/r. However, let us observe that if $\dot{r} = \dot{z} = 0$ we have that $H_{\mathcal{C}+\mathcal{R}} = V(r,z)$, so V still plays the role of an effective potential (its saddle being a barrier between bounded and unbounded motions). The associated Hamilton's equations of motion do not possess simple restricted solutions if $J_{\mathcal{R}} \neq 0$ or $J_{\mathcal{C}} \neq 0$ (as those discussed in Section 4.2 for system $\mathcal{C}$), but we can also define a *trapping region* whenever $J_{\mathcal{C}} \neq 0$.

Indeed, the potential does not depend on $J_{\mathcal{R}}$, and hence the properties of the motion which can be derived from the qualitative properties of $V(r,z)$ are the same as for the single circular wire. Let us summarise them in the following list. For more details see Section 4.3.

1. Provided that $L_0 > 0$, the Hamiltonian defined by Eq. (28) has a global minimum on the curve $\Gamma_{L_0} := \{J_{\mathcal{C}} I(r,z) + L_0 = 0, p_r = \frac{2J_{\mathcal{R}} z}{r}, p_z = 0\}$ and the level sets of H near Γ_{L_0} are compact submanifolds.

2. The saddle point $(r_M, 0)$ and the escape energy $E_{\text{escape}} := V(r_M, 0)$ are independent of the value of $J_{\mathcal{R}}$. In particular, their dependence on L_0 is the same as for system $\mathcal{C}$, e.g. see Fig. 2(b) for the case $J_{\mathcal{C}} = 1$.

3. The region of allowed motions is given by $\{V(r,z) \leq H_0\} \times \mathbb{S}^1$. For $L_0 > 0$ there is a *trapping region* which is defined by the bounded component of the set $\{V(r,z) < E_{\text{escape}}\} \times \mathbb{S}^1$. When $L_0 \leq 0$ all the connected components of $\{V(r,z) \leq H_0\}$ are non-compact, and hence most of the motions are unbounded.

When $J_{\mathcal{R}} = 0$ we showed in Section 4.3 the existence of many periodic and quasi-periodic solutions of (13) near the minimum Γ_{L_0}. The main difference with the general case $J_{\mathcal{R}} \neq 0$ is that the reduced Hamiltonian (28) still has a magnetic term $\frac{2J_{\mathcal{R}} z}{r}$. This occurs because the magnetic field $B_{\mathcal{C}+\mathcal{R}}$ has an angular component $B_\phi = \frac{2J_{\mathcal{R}}}{r^2}$. If one applies Braun's technique it is easy to realize that the extra term cannot be considered as a small perturbation after the symplectic change (19) and the scaling used in the proof of Theorem 4.3, unless $J_{\mathcal{R}}/J_{\mathcal{C}} \ll 1$. It is worth mentioning that the case $B_\phi \neq 0$ was treated by Castilho in [13], where a criterion for the existence of quasi-periodic solutions was obtained. Regretfully, one of the assumptions is that the level sets of B_ϕ in the (r,z) half-plane must be compact curves, a property which is not fulfilled in our problem. Following Braun's approach, we can state the following result:

Proposition 5.1. *Set $J_{\mathcal{C}} = 1$ and $J_{\mathcal{R}} = \delta/2$. For any value of $L_0 > 0$ there exist periodic and quasi-periodic solutions of the Hamiltonian system defined by Eqs.* (28) *and* (29) *at a distance ε of Γ_{L_0}, provided that δ is of order at most ε^3.*

Proof. The Hamiltonian (28) can be written as

$$H_{\mathcal{C}+\mathcal{R}}(r,z,p_r,p_z) = \frac{1}{2}p_r^2 + \frac{1}{2}p_z^2 + V(r,z) + \delta P_0(r,z,p_r,p_z)\,,$$

where $P_0(r,z,p_r,p_z) := \frac{\delta z^2}{2r^2} - \frac{z p_r}{r}$. Note that the term of $H_{\mathcal{C}+\mathcal{R}}$ which does not depend on δ is the Hamiltonian H of the single circular wire, cf. Eq. (13). Let us now change coordinates and introduce the scale parameter ε as in Section 4.3. The transformation is $(r,z,p_r,p_z) \to (X,Y,p_X,p_Y)$, and a new Hamiltonian $H^\varepsilon_{\mathcal{C}+\mathcal{R}} := \varepsilon^{-2} H_{\mathcal{C}+\mathcal{R}}$ is defined, thus obtaining

$$H^\varepsilon_{\mathcal{C}+\mathcal{R}} = \frac{1}{2}a(\varepsilon X)p_X^2 + \frac{1}{2}b(\varepsilon X)p_Y^2 + \frac{1}{2}c(\varepsilon X)Y^2 + \varepsilon g(X,Y,p_X,p_Y;\varepsilon) + \frac{\delta}{\varepsilon^2}P(X,Y,p_X,p_Y;\varepsilon)\,.$$

In this equation the terms a, b, c, g are the functions defined in Section 4.3, and P is just the transformed of P_0 under the change of coordinates. As the parameter δ is independent of the scale ε, we can set $\delta = \varepsilon^3$, which just means that when we study solutions which are ε-close to

Γ_{L_0}, the intensity current of $\mathcal{R}$ is assumed to be ε^3-small. In this case the Hamiltonian takes the form

$$H^{\varepsilon}_{\mathcal{C}+\mathcal{R}} = \frac{1}{2}a(\varepsilon X)p_X^2 + \frac{1}{2}b(\varepsilon X)p_Y^2 + \frac{1}{2}c(\varepsilon X)Y^2 + \varepsilon(g+P)(X,Y,p_X,p_Y;\varepsilon)\,,$$

and hence the perturbation term is now of order ε. Proceeding as in the proof of Theorem 4.3 we can rewrite the non-perturbative term of this Hamiltonian (which is exactly the same as in Section 4.3) and compute its Poincaré map for a suitably chosen Poincaré section. This map turns out to be of twist type (with one small frequency), and Moser's twist theorem can be applied, thus concluding the existence of quasi-periodic solutions. Periodic solutions follow from Poincaré-Birkhoff theorem, as in Corollary 4.5. Details are analogous to those given in Section 4.3. □

According to numerical experiments (that are provided in Section 6), if we take $J_{\mathcal{C}} \simeq J_{\mathcal{R}}$ there are still many quasi-periodic solutions near Γ_{L_0}. However, we have not been able to perform a change of coordinates that writes the Hamiltonian in a neighbourhood of the curve of fixed points in a suitable way to apply Moser's twist theorem.

It is clear that system $\mathcal{C}+\mathcal{R}$ can be used to construct magnetic traps, as in the case of the single circular wire, for details consult Section 4.4. The mechanism is exactly the same: we increase the current intensity $J_{\mathcal{C}}$ and accordingly the escape energy also increases, thus confining some particles in the new trapping region. Observe that this phenomenon does not depend on the value of $J_{\mathcal{R}}$. Outside the confinement region all solutions are of scattering type, as will be numerically illustrated in Section 6.

Let us finally prove that $|z(t)|/r(t)$ cannot remain bounded for scattering solutions of the Hamiltonian system (28). This property is quite intuitive because as r increases the contribution of the magnetic field of the infinite filament (of order r^{-1}) is much bigger than the contribution of the magnetic field of the circular wire (of order r^{-3}). Roughly speaking, when r is big enough the dynamics is dominated by the rectilinear current, and therefore $r(t)/z(t)$ cannot grow indefinitely as proved in Section 3. Actually, numerical computations show that the r coordinate is always bounded. This is an important difference with the case of the single circular wire, which has many scattering trajectories escaping to infinity on the invariant plane $\{z=0\}$ in the r direction, as we proved in Section 4.2. In the next section we shall study in more detail the scattering properties of system $\mathcal{C}+\mathcal{R}$ using numerics.

Proposition 5.2. *Assume that $L_0 > 0$. For any scattering solution of the Hamiltonian system defined by Eqs.* (28) *and* (29) *we have that $\frac{|z(t)|}{r(t)}$ is not uniformly bounded in t, provided that H_0 is large enough.*

Proof. The Newton-Lorentz equations associated to this system read as

$$\ddot{r} = -\frac{2J_{\mathcal{R}}\dot{z}}{r} + \frac{(L_0 + J_{\mathcal{C}}I(r,z))^2}{r^3} - \frac{J_{\mathcal{C}}(L_0+I(r,z))\partial_r I(r,z)}{r^2}\,, \tag{30}$$

$$\ddot{z} = \frac{2J_{\mathcal{R}}\dot{r}}{r} - \frac{J_{\mathcal{C}}(L_0+I(r,z))\partial_z I(r,z)}{r^2}\,. \tag{31}$$

Let us fix $L_0 > 0$ and $H_0 > 0$, and assume that there is a scattering solution $(r(t), z(t))$ to these equations such that $\frac{|z(t)|}{r(t)} \leq C_0$ for some positive constant C_0 and for all $t \geq 0$. Note that, on account of the conservation of energy, $V(r(t), z(t)) \leq H_0$ and hence $r(t) \geq C_1$ for all t, thus implying that $\lim_{t\to\infty} r(t) = \infty$ and $|z(t)|$ is uniformly bounded in t or it tends to infinity no faster than $r(t)$.

Now set $q := (r, z)$ and observe that

$$\frac{d^2}{dt^2}\Big(\frac{|q|^2}{2}\Big) = \dot{q}\cdot\dot{q} + q\cdot\ddot{q}\,. \tag{32}$$

Using that $\lim_{t\to\infty} V(r(t), z(t)) = 0$ because of the asymptotic properties of the potential we have that for every $\delta_0 > 0$ there exists $T > 0$ big enough such that $V(r(t), z(t)) \leq \delta_0$ for $t \geq T$. Therefore

$$\dot{q}\cdot\dot{q} = (p_r - 2J_{\mathcal{C}} z/r)^2 + p_z^2 = 2H_0 - V(q) \geq 2H_0 - \delta_1\,, \tag{33}$$

with $\delta_1 := 2\delta_0$. On the other hand, $q\cdot\ddot{q} \geq -|q||\ddot{q}|$, and using the expressions (30) and (31) for $\ddot{r}$ and $\ddot{z}$ we get

$$q\cdot\ddot{q} \geq -|q|\sqrt{\frac{4J_{\mathcal{R}}^2|\dot{q}|^2}{r^2} + O(|q|^{-3})} = -\frac{2J_{\mathcal{R}}|q||\dot{q}|}{r} + O(|q|^{-1/2}) \geq -C_2|\dot{q}| + \delta_2\,, \tag{34}$$

where we have taken into account that $\frac{|q|}{r} \leq 1 + \frac{|z|}{r}$ is bounded uniformly in t by assumption, and that $|q|$ is as big as we want if $t \geq T$. Introducing Eqs. (33) and (34) into Eq. (32) we obtain

$$\frac{d^2}{dt^2}\Big(\frac{|q|^2}{2}\Big) \geq 2H_0 - C_2|\dot{q}| + \delta_3\,.$$

This inequality can be written in a different way just noting that

$$|\dot{q}| = \sqrt{\dot{r}^2 + \dot{z}^2} \leq \sqrt{2H_0} + \delta_4\,,$$

provided that $t \geq T$. This allows us to conclude that

$$\frac{d^2}{dt^2}\Big(\frac{|q|^2}{2}\Big) \geq 2H_0 - C_2\sqrt{2H_0} + \delta_5\,,$$

and therefore, provided that H_0 is sufficiently large, we get

$$\frac{d^2}{dt^2}\Big(\frac{|q|^2}{2}\Big) \geq C_3\,,$$

for some positive constant C_3. Integrating this equation twice we finally obtain a lower bound for the growth of $|q(t)|$, which is linear in t, that is

$$|q(t)| \geq C_4 t \tag{35}$$

if $t \geq T$. This is the key property to prove that the assumption $\frac{|z(t)|}{r(t)} \leq L_0$ cannot hold. Indeed, let us integrate Eq. (31):

$$\dot{z}(t) = P_0 + 2J_{\mathcal{R}} \ln r(t) - \int_0^t \frac{J_{\mathcal{C}}(L_0 + I(r(t), z(t)))\partial_z I(r(t), z(t))}{r(t)^2} dt \,,$$

with $P_0 := \dot{z}_0 - 2J_{\mathcal{R}} \ln r_0$. The integral in this equation can be bounded from above when $t \geq T$ by

$$\int_T^t \frac{J_{\mathcal{C}}(L_0 + I(r(t), z(t)))\partial_z I(r(t), z(t))}{r(t)^2} dt \leq C_5 \int_T^t \frac{|z(t)|dt}{[r(t)^2 + z(t)^2]^{5/2}} \,,$$

where we have used the asymptotic expansion of $\partial_z I(r, z)$, cf. the proof of Lemma 4.7, and the fact that $\lim_{t\to\infty} I(r(t), z(t)) = 0$. Noticing that $\frac{d|z(t)|}{dt} \leq |\dot{z}| \leq \sqrt{2H_0}$ it follows that $|z(t)| \leq C_6 t$, and taking into account the estimate (35) we can write

$$\dot{z}(t) \geq P_0 + 2J_{\mathcal{R}} \ln r(t) + C_7 - \frac{C_5 C_6}{C_4^5} \int_T^t \frac{dt}{t^4} \,,$$

where the constant C_7, positive or negative, is just a transient quantity which represents the value of the integral till time $t = T$. Being the last integral convergent when $t \to \infty$, the fact that $\lim_{t\to\infty} r(t) = \infty$ implies that $\lim_{t\to\infty} \dot{z}(t) = \infty$. But this contradicts the conservation of the energy and hence the claim of the proposition follows. □

6 Numerical studies

In this section we explore numerically the systems $\mathcal{C}$ and $\mathcal{C} + \mathcal{R}$ in order to obtain more information on the global dynamics in both problems. Due to the axial symmetry, it is enough to consider the reduced motions on the (r, z) half-plane given by Eqs. (13) and (14) for system $\mathcal{C}$ and Eqs. (28) and (29) for system $\mathcal{C} + \mathcal{R}$.

As discussed in Sections 4.3 and 5, in these systems we can define a trapping region with bounded dynamics, which corresponds to initial conditions with energy below a threshold value E_{escape}. In Section 6.1 we describe the dynamics in the interior of this region by computing Poincaré sections and Lyapunov exponents. Beyond the threshold, i.e. when the energy permits to escape from the saddle, we obtain an open Hamiltonian system that is analysed in Section 6.2 by computing fractal basins of scattering trajectories and their fractal dimensions.

All computations have been performed using a C++ compiler whereas evaluation of complete elliptic integrals has been provided by the routines `gsl_sf_ellint_Kcomp` and `gsl_sf_ellint_Ecomp` of GSL-GNU (see [18]). To integrate the different systems of equations we have used a 8/9th order Runge-Kutta Prince-Dormand method provided by `gsl_odeiv_step_rk8pd`. All along this section we will assume that $2J_{\mathcal{R}} = J_{\mathcal{C}} = 1$.

6.1 Bounded motions: invariant tori and chaos

The standard approach for monitoring the dynamics of a 2DOF Hamiltonian system is to compute a reduced Poincaré section. To this end, let us introduce some notation that will be useful later on. Given a fixed value of $L_0 > 0$ we consider the *Poincaré section* Σ_{L_0,H_0} given by the hyperplane $\{z = 0\}$ and the energy H_0, which we parametrise by means of (r, p_r). Let us denote by $P_{L_0,H_0} : \Sigma_{L_0,H_0} \mapsto \Sigma_{L_0,H_0}$ the Poincaré map at energy H_0 defined in the usual way.

In Fig. 6 we show several sections for the systems $\mathcal{C}$ and $\mathcal{C} + \mathcal{R}$. For each picture we have computed 10000 iterates of P_{L_0,H_0} for 100 different initial conditions (in the plots many iterates are skipped in order to reduce the size of the figure). In these computations we ask for tolerances 10^{-15} both in the local integration error and in the intersection with the section. The final integration time for each orbit ranges from $2 \cdot 10^4$ up to $1.2 \cdot 10^5$ time units. For $L_0 = 4$, we observe that at low energy —see Fig. 6(a)-(b)— some invariant tori in system $\mathcal{C}$ breakdown due to the presence of the straight line wire in system $\mathcal{C} + \mathcal{R}$. However, for a higher energy —see Fig. 6(c)-(d)— the difference in the behaviour of these systems is not so evident. For this reason, in order to describe the complexity of the motions, we resort to quantitative computations based on Lyapunov exponents.

Lyapunov exponents give information about how fast nearby orbits separate (they measure the hyperbolicity in the vicinity of an orbit) so they are regarded as indicators of the existence of sensitive dependence with respect to initial conditions, and hence, to some amount of unpredictability and chaos. It is well known that their computation requires to approximate a limit whose convergence is very difficult to ensure in practice. For example, a given trajectory can start close to an invariant torus (which has zero maximal Lyapunov exponent) and then, perhaps after a big time interval, drift to a chaotic region. For this reason, they have to be understood as local indicators of the dynamics both in space coordinates and time. Therefore, in order to obtain a global picture of the dynamics inside the region of bounded motions, we perform an extensive computation of Lyapunov exponents sampling big regions of phase space, in order to estimate the *fraction of stability* (fraction of volume occupied by invariant tori). To this end, we follow valuable ideas given in [37]. It is worth mentioning that the first computations related to the volume of tori appeared more than 40 years ago in the pioneering work of Hénon and Heiles [20].

For convenience, let us recall the basic ideas regarding the computation of the maximal Lyapunov exponent. Given an n-dimensional system $\dot{x} = X(x)$, a point $x_0 \in \mathbb{R}^n$ and a vector $v_0 \in \mathbb{R}^n$, the maximal Lyapunov exponent is given by

$$\Lambda = \lim_{t\to\infty} \frac{1}{t} \log \frac{|v(t, v_0)|}{|v_0|},$$

where $v(t, v_0)$ is the solution of the variational equation around the trajectory satisfying $x(0) = x_0$, i.e. $\dot{v} = DX(x)v$, with $v(0) = v_0$. Obviously, Λ does not depend on the point x_0 but on its orbit. To approximate the above limit we select $v_0 = (1, 0, \ldots, 0)$ and integrate the equation up to time Δt to compute $\bar{v}_1 := v(\Delta t, v_0)$, $\lambda_1 := \log |\bar{v}_1|$ and $v_1 := \bar{v}_1/|\bar{v}_1|$. Then, we compute

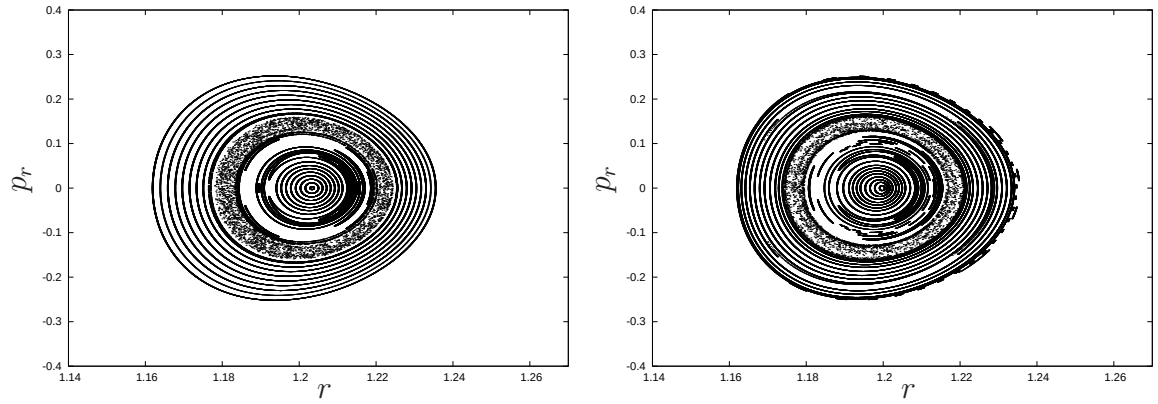

(a) System $\mathcal{C}$ with $H_0 = 0.05E_{\text{escape}}$.

(b) System $\mathcal{C} + \mathcal{R}$ with $H_0 = 0.05E_{\text{escape}}$.

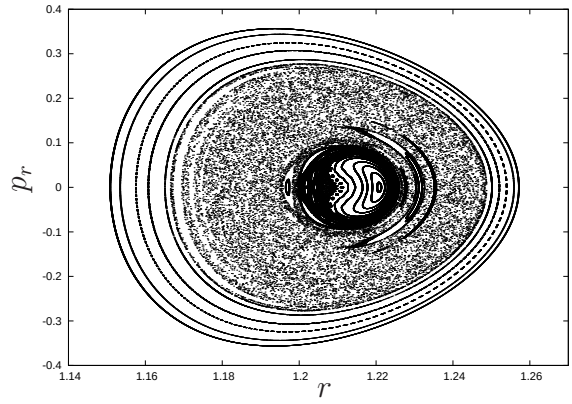

(c) System $\mathcal{C}$ with $H_0 = 0.1E_{\text{escape}}$.

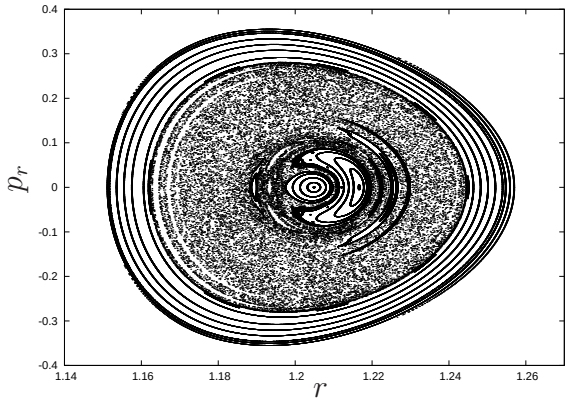

(d) System $\mathcal{C} + \mathcal{R}$ with $H_0 = 0.1E_{\text{escape}}$.

Figure 6: Poincaré sections for systems $\mathcal{C}$ and $\mathcal{C} + \mathcal{R}$ using $L_0 = 4$. In this case $E_{\text{escape}} = 0.635247$.

recursively

$$\lambda_m = \lambda_{m-1} + \log(|\bar{v}_m|), \qquad \Lambda_m = \frac{\lambda_m}{m\Delta t},$$

where $\bar{v}_m := v(\Delta t, v_{m-1})$ and $v_m := \bar{v}_m/|\bar{v}_m|$, so it turns out that $\Lambda = \lim_{m\to\infty} \Lambda_m$. As a criterion for convergence we check the following

$$\max\{|\Lambda_{m-2s} - \Lambda_{m-s}|, |\Lambda_{m-s} - \Lambda_m|, |\Lambda_{m-2s} - \Lambda_m|\} \leq \delta$$

and then we take the average of these three values. The computations presented in this paper have been obtained using $\Delta t = 5$, $s = 50$ and $\delta = 10^{-4}$.

If we want to compute Lyapunov exponents in a big region of phase space we can save many computations using the fact that points on the same orbit have the same exponent. To this end,

we discretize a Poincaré section Σ_{L_0,H_0} by means of a grid of pixels and compute the maximal Lyapunov exponent for initial conditions falling on these pixels, taking into account that we can associate the same exponent to those pixels where the same orbits falls. Let us remark that some of these pixels may contain points of different dynamical properties, but if they are small enough, we will reflect statistically the dominant character of every pixel. For the sake of reproducibility of our computations, we describe next the implementation of the previous ideas:

1. We fix a value of $L_0 > 0$ and compute the saddle point r_M from Eq. (17) and also the escape energy $E_{\text{escape}} = V(r_M, 0)$.

2. We fix an energy $H_0 < E_{\text{escape}}$ and we set a rectangle such that

$$\Sigma_{L_0,H_0} \subset [r^{\min}, r^{\max}] \times [p_r^{\min}, p_r^{\max}].$$

   $r^{\min}, r^{\max}$ are the the minimum and maximum values of r which solve the equation $V(r, 0) = H_0$ for $r < r_M$, and we set $p_r^{\min} = -\sqrt{2H_0}$ and $p_r^{\max} = \sqrt{2H_0}$. Then, we discretize this rectangle by means of a grid of $N \times N$ pixels.

3. We define the matrix `grid[N][N]` of integer numbers where we will store a `0` if the pixel has not been studied, `1` if the pixel has been used as an initial condition for computing a Lyapunov exponent and `2` if the orbit of a previously studied initial condition fell into this pixel. We set the value `-1` if the pixel is not allowed (according to the energy). The relation between a pixel `[i][j]` and the corresponding initial condition $(r^{(i)}, p_r^{(j)})$ on Σ_{L_0,H_0} is obtained from the expressions

$$\texttt{i} = \left\lfloor \frac{r^{(i)} - r^{\min}}{r^{\max} - r^{\min}} N \right\rfloor, \qquad \texttt{j} = \left\lfloor \frac{p_r^{(j)} - p_r^{\min}}{p_r^{\max} - p_r^{\min}} N \right\rfloor,$$

   where $\lfloor \cdot \rfloor$ stands for the integer part.

4. We define the matrix `where_r[N][N]` of integer numbers that allows us to find the r component of the original pixel whose orbit has fallen into the pixel `[i][j]` (this makes sense if `grid[i][j]=2`). In particular, if for the initial condition $(r^{(k)}, p_r^{(l)})$ on the pixel `[k][l]` there exists $n \in \mathbb{N}$ such that $P^n_{L_0,H_0}(r^{(k)}, p_r^{(l)})$ falls into the pixel `[i][j]`, then we set `where_r[i][j]=k`. Analogously, we define the matrix `where_pr[N][N]` associated to the p_r component.

5. We proceed by scanning all the pixels in the discretization of Σ_{L_0,H_0} by skipping all points whose character has already been decided, i.e., such that `grid[i][j]` is different from `0`. Then, while computing the exponent associated to a pixel we update the matrices `grid[N][N]`, `where_r[N][N]` and `where_pr[N][N]` according to the Poincaré map.

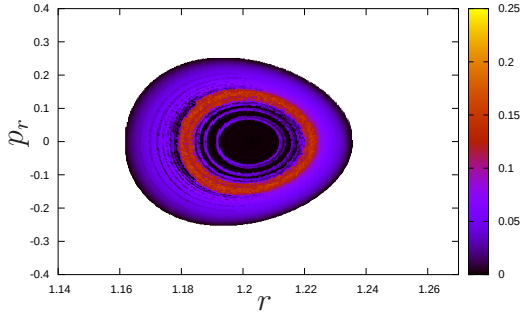

(a) System $\mathcal{C}$ with $H_0 = 0.05E_{\text{escape}}$.

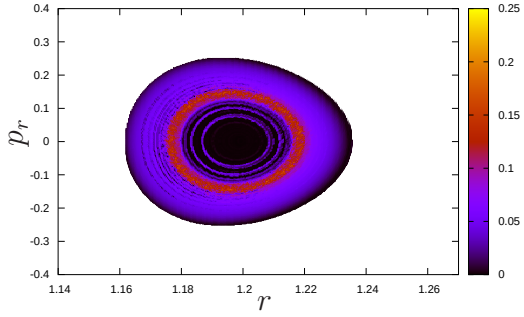

(b) System $\mathcal{C} + \mathcal{R}$ with $H_0 = 0.05E_{\text{escape}}$.

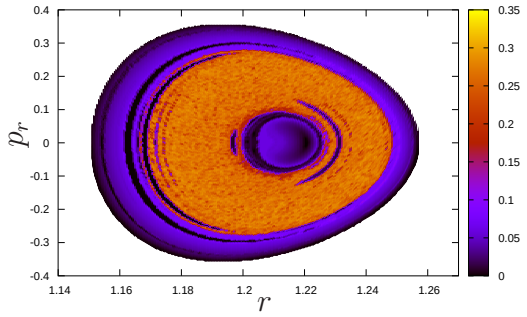

(c) System $\mathcal{C}$ with $H_0 = 0.1E_{\text{escape}}$.

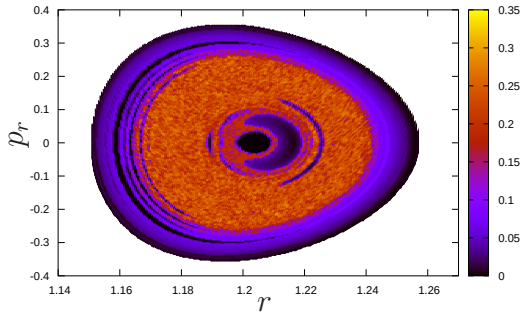

(d) System $\mathcal{C} + \mathcal{R}$ with $H_0 = 0.1E_{\text{escape}}$.

Figure 7: Maximal Lyapunov exponents Λ for systems $\mathcal{C}$ and $\mathcal{C} + \mathcal{R}$ using $L_0 = 4$. In this case $E_{\text{escape}} = 0.635247$.

6. We store the computed Lyapunov exponents in the matrix `lyap[N][N]`. On the one hand, if `grid[i][j]` contains `1`, we store the Lyapunov exponent computed using the initial condition $(r^{(i)}, p_r^{(j)})$ as described above. On the other hand, if `grid[i][j]` contains `2`, we store `lyap[where_r[i][j]][where_pr[i][j]]`.

7. Finally, we define N_0 as the number of pixels such that the Lyapunov exponent is less than 0.01 and we estimate the fraction of stability as $f_s = N_0/N_1$, where N_1 is the total number of allowed pixels (note that N_1 depends on the energy H_0).

Figure 7 represents the Lyapunov exponents Λ corresponding to initial conditions $(r, p_r) \in \Sigma_{L_0,H_0}$ in a colour chart from black (when $\Lambda = 0$) to yellow (maximum value Λ in the dis-

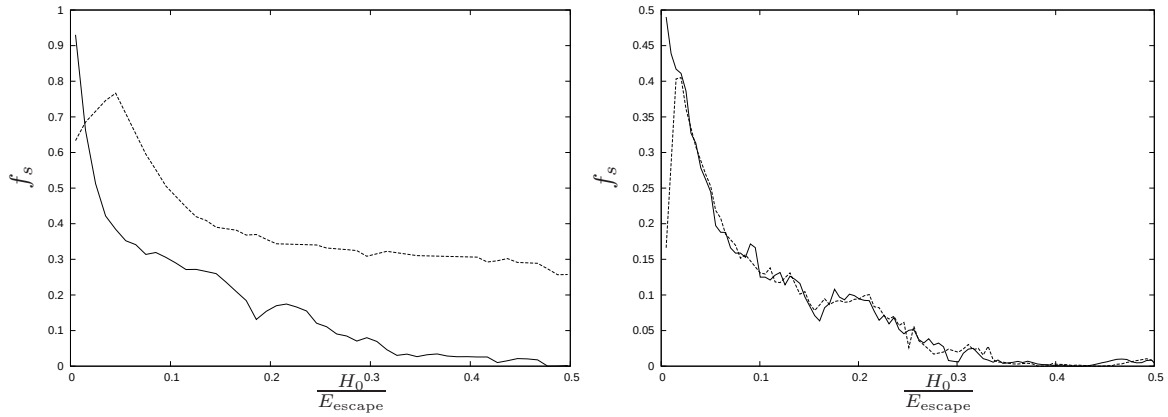

(a) $L_0 = 2$ (b) $L_0 = 4$

Figure 8: Fraction of stability f_s versus energy for system $\mathcal{C}$ (solid line) and system $\mathcal{C} + \mathcal{R}$ (dashed line). In the horizontal axis we show the energy of the system scaled as H_0/E_{escape}.

cretization of Σ_{L_0,H_0}) and using a grid of 256×256 pixels as has been described. The four pictures correspond to the Poincaré sections of Fig. 6, and we can observe the good agreement between the observed objects in Fig. 6 (invariant tori or chaotic zones) and the coloured regions in Fig. 7.

Figure 8 plots the fraction of stability f_s for both systems $\mathcal{C}$ and $\mathcal{C} + \mathcal{R}$ as a function of the energy H_0/E_{escape} (it is convenient to scale the energy according to the escape energy) for $L_0 = 2$ and $L_0 = 4$. Let us make some observations:

1. High energy: for $L_0 = 2$ and $H_0/E_{\text{escape}} > 0.014$, system $\mathcal{C}$ presents a smaller fraction of stability than $\mathcal{C} + \mathcal{R}$. When increasing the angular momentum to $L_0 = 4$, it turns out that for all energies after a threshold value, both systems $\mathcal{C}$ and $\mathcal{C} + \mathcal{R}$ show the same chaoticity. In fact, if we performed the same computations for $L_0 = 6$, we would observe that both systems show a totally indistinguishable complexity for all energies. This is due to the fact that when L_0 is increased, bounded trajectories in system $\mathcal{C} + \mathcal{R}$ move away from the infinite rectilinear filament $\mathcal{R}$ and its influence on them decreases substantially (r_M decreases with L_0, cf. Fig. 2(b), and hence the trapping region becomes closer to $\mathcal{C}$).

2. Low energy: contrary to what one could expect, for $H_0/E_{\text{escape}} < 0.014$ we have that for system $\mathcal{C} + \mathcal{R}$ the fraction of stability decreases when H_0 decreases. This fact must be carefully analysed in order to avoid false conclusions. For example, for $L_0 = 4$ and $H_0/E_{\text{escape}} = 0.005$ it turns out that the *orange* chaotic ring observed in Fig. 7(a)-(b) becomes very narrow and the trajectories inside the corresponding closed region have a typical Lyapunov exponent of 0.0008 for system $\mathcal{C}$ and 0.013 for system $\mathcal{C}+\mathcal{R}$. According to our convention, those trajectories of system $\mathcal{C} + \mathcal{R}$ do not contribute to f_s (because

$0.013 > 0.01$), even though they have a very small Lyapunov exponent. Nevertheless, since the Lyapunov exponents associated to the system $\mathcal{C} + \mathcal{R}$ are larger than those of $\mathcal{C}$ for small H_0/E_{escape}, we can state that at low energy, the former system is more complex than the latter.

6.2 Unbounded motions: chaotic scattering

Chaotic scattering can be understood as the interaction of a particle with a system that scatters it in a way that, after leaving the vicinity of the system, the final dynamical conditions of the particle (e.g. speed and direction) depend sensitively on its initial conditions [8, 5]. This phenomenon is associated to the existence of a compact chaotic invariant set (or chaotic saddle), i.e. a null-measure set of infinitely many unstable periodic (of every period) and aperiodic orbits. The region where the particle bounces erratically for a certain time is usually called *scattering region*.

In this section we shall study the scattering of charged particles that enter into the trapping regions of systems $\mathcal{C}$ and $\mathcal{C} + \mathcal{R}$. The tools will be the typical ones in chaotic scattering: *exit basins* to get a qualitative idea of the predictability associated to these systems, and the *uncertainty dimension* to quantitatively measure their fractality. Let us observe that only trajectories with $L_0 > 0$ show some complexity, and therefore in this section we shall focus exclusively on this regime.

Computation of fractal basins

Figure 9 shows the level curves of the potential $V(r, z)$ for $L_0 = 4$, cf. Eq. (14). For energies $H_0 < E_{\text{escape}}$, case studied in Section 6.1, there are two regions, one with bounded orbits and the other one with regular scattering. For energies $H_0 > E_{\text{escape}}$, one exit appears and chaotic scattering becomes possible, so we will assume this case in what follows. Let us observe that the Hamiltonian (28) of the coupled system $\mathcal{C} + \mathcal{R}$ is not natural because it contains a magnetic term, but as discussed in Section 5, the function $V(r, z)$ can be still interpreted as an effective potential, so that systems $\mathcal{C}$ and $\mathcal{C} + \mathcal{R}$ share the same exit and escape energy. This fact makes the comparison between both systems especially fruitful.

We recall that the exit basin associated to an exit $\mathcal{E}$ of a dynamical system is defined as the set of initial conditions that escape from the scattering region through the exit $\mathcal{E}$. When the exit basin boundaries are smooth, the system is said to be non-fractal, while fractal exit basin boundaries are associated to systems exhibiting chaotic scattering.

In our case, the scattering region is the vicinity of the circular wire, and the trajectories can escape towards infinity through only one exit (see Fig.9(c)). For systems with one exit we can create *artificial exits* in order to be able to plot the exit basins [5]. In our particular problem, we fix $L_0 > 0$ and we select an energy $H_0 > E_{\text{escape}}$. Then, we fix a suitable $R_{\text{escape}} > r_M$ and we say that a trajectory $(r(t), z(t))$ escapes from the scattering region if there exists an *escape time* $t_{\text{escape}} > 0$ such that $r(t_{\text{escape}}) = R_{\text{escape}}$ and $\dot{r}(t_{\text{escape}}) > 0$. In addition, we define the artificial

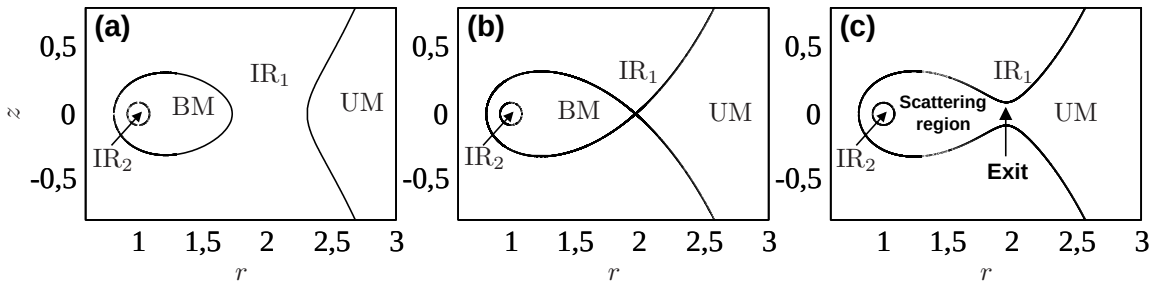

Figure 9: Level curves of the potential $V(r,z)$ for $L_0 = 4$. (a) $H_0 = 0.6 < E_{\rm escape}$, (b) $H_0 = 0.635247 = E_{\rm escape}$, and (c) $H_0 = 1 > E_{\rm escape}$. For every value of the energy, the (r,z) half-plane shows two inaccessible regions (IR_1 and IR_2). For energies $H_0 \leq E_{\rm escape}$ there is one region with bounded motion (BM) and one with unbounded motion (UM), and these two regions collide for $H_0 = E_{\rm escape}$ and become an open region for $H_0 > E_{\rm escape}$ with one exit where chaotic scattering is possible.

exits as follows: we assign the colour green if $z(t_{\rm escape}) \geq 0$ and the colour red otherwise. We have to take into account that all orbits in system $\mathcal{C}+\mathcal{R}$ escape to infinity with positive values of z, which means that all conditions that are plotted in red for this system will eventually turn upwards and cross $z = 0$. Therefore, we have to select $R_{\rm escape}$ sufficiently close to r_M in order to obtain an accurate picture of the dynamics.

Figure 10 shows the exit basins for system $\mathcal{C}$ and Fig. 11 shows the exit basins for system $\mathcal{C}+\mathcal{R}$, for several values of the energy. We have taken $L_0 = 4$ (in this case the escape energy is $E_{\rm escape} \simeq 0.635247$) and $R_{\rm escape} = 2$ (the saddle is at $r_M \simeq 1.971505$). We characterize initial conditions by fixing $z = 0$, an energy H_0, a value of r and a *shooting angle* θ on the half-plane $(r,z) \in \mathbb{R}^+ \times \mathbb{R}$ (where $\theta = 0$ points in the positive direction of the r-axis). We scan 500×500 initial conditions corresponding to $(r,\theta) \in [0.8, 2.5] \times (0, 2\pi)$. The initial conditions plotted white either do not have any trajectories associated or correspond to orbits that do not escape from the scattering region, even if they have enough energy to do so (they are trapped in the interior of invariant tori). Let us summarise the main properties of the exit basins:

1. In both systems it is observed that higher values of the energy make the structures less fractal, as is typical in open Hamiltonian systems. We will analyse this fact in a quantitative way when we calculate the fractal dimension of the exit basin boundaries.

2. Invariant tori are present for some values of the energy in both systems $\mathcal{C}$ and $\mathcal{C}+\mathcal{R}$. For instance, in system $\mathcal{C}$ we have detected an invariant torus for $H_0 \in (0.95, 1.21)$, and therefore it can be seen plotted in white in Fig. 10(c).

3. System $\mathcal{C}$ is reversible[1] with respect to the classical involution

$$\Theta(r, z, p_r, p_z) = (r, z, -p_r, -p_z)\,,$$

[1]Let us recall that a system $\dot{x} = X(x)$ is reversible if there exists an involution $x = \Theta(y)$ (i.e., a change of

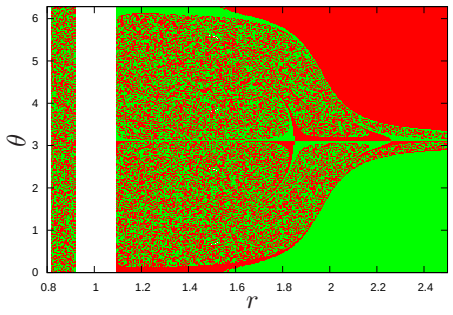

(a) $H_0 = 0.64 = 1.01E_{\text{escape}}$

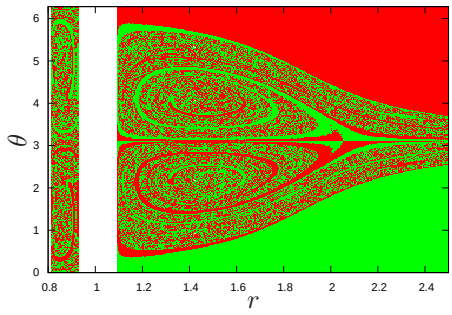

(b) $H_0 = 0.7 = 1.1E_{\text{escape}}$

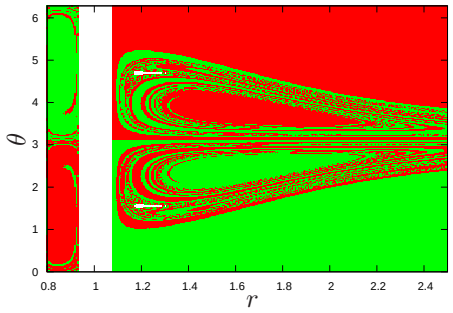

(c) $H_0 = 1 = 1.57E_{\text{escape}}$

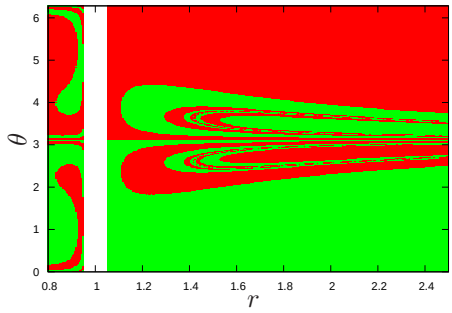

(d) $H_0 = 2.5 = 3.94E_{\text{escape}}$

Figure 10: Fractal exit basins for several energies for system $\mathcal{C}$ and $L_0 = 4$. Exit 1 ($r = R_{\text{escape}}$, $\dot{r} > 0$, $z \geq 0$) is plotted green, exit 2 ($r = R_{\text{escape}}$, $\dot{r} > 0$, $z < 0$) is plotted red and initial conditions that do not give rise to orbits (vertical stripes around $r = 0.8$ and $r = 1$) or do not escape are plotted white (see zones in (c) that correspond to invariant tori).

and this explains the symmetry with respect to $\theta = \pi$ of the basins of system $\mathcal{C}$ (see Fig. 10). On the other hand, system $\mathcal{C} + \mathcal{R}$ is not reversible with respect to the previous involution so we cannot derive the same symmetry for its fractal boundaries. Nevertheless, it is reversible with respect to the involution $\Theta(r, z, p_r, p_z) = (r, -z, -p_r, p_z)$, thus implying that a similar symmetry can be obtained using other coordinates.

variables satisfying $\Theta^2 = \text{id}$ and $\Theta \neq \text{id}$) such that $\dot{y} = D\Theta^{-1}(y)X(\Theta(y)) = -X(y)$. One of the dynamical consequences of reversibility is that if $x(t)$ is a solution, then so is $\Theta(x(-t))$.

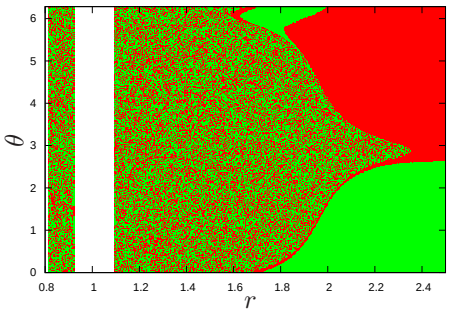

(a) $H_0 = 0.64 = 1.01E_{\text{escape}}$

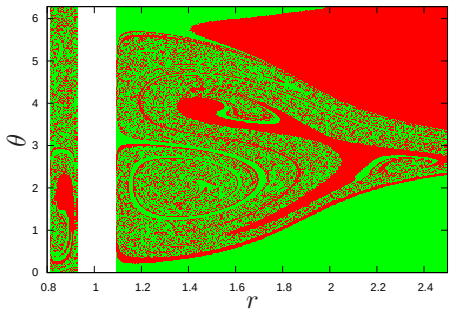

(b) $H_0 = 0.7 = 1.1E_{\text{escape}}$

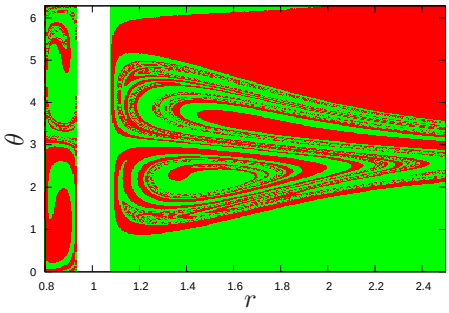

(c) $H_0 = 1 = 1.57E_{\text{escape}}$

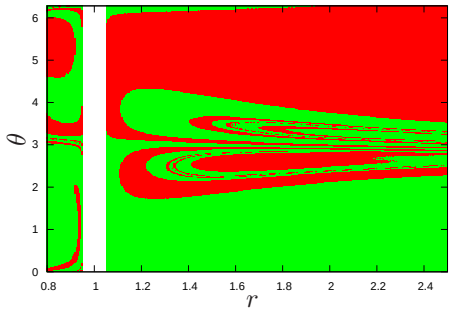

(d) $H_0 = 2.5 = 3.94E_{\text{escape}}$

Figure 11: Fractal exit basins for several energies for system $\mathcal{C} + \mathcal{R}$ and $L_0 = 4$. Exit 1 is plotted green, exit 2 is plotted red and initial conditions that do not give rise to orbits (vertical stripes around $r = 0.8$ and $r = 1$) are plotted white.

4. Other important difference between both systems is obtained comparing Fig. 10(a) and Fig. 11(a). In system $\mathcal{C}$, no matter how far away we are from the scattering region (i.e. how large is r_0), for $z_0 = 0$ and initial shooting angle $\theta_0 \approx \pi$, the particle can always cross the exit of the system in the inner direction, spend some time bouncing erratically in the scattering region and then escape towards infinity suffering chaotic scattering. On the contrary, in Fig. 11(a) we can observe that for $z = 0$ and $r > 2.35$ fractality disappears and the scattering is not chaotic anymore. In fact, what happens is that if r_0 is big enough, the particle will turn upwards and escape to $z \to \infty$ without even entering the scattering region.

Computation of fractal dimension

The fractal dimension is the object that measures the complexity of a fractal basin boundary. While there are several definitions of fractal dimension, the most convenient for chaotic scattering problems is the uncertainty dimension [25], which is known to coincide with the box-counting dimension in typical dynamical systems.

The uncertainty dimension of an exit basin boundary for a dynamical system $\dot{x} = X(x)$, $x \in \mathbb{R}^N$, is defined as follows. Given an initial condition x_0, we label it as *certain* if the neighbouring initial conditions escape through the same exit, and we label it as *uncertain* otherwise. Moreover, given a tolerance ε in the determination of initial conditions, we consider $f(\varepsilon)$ as the fraction of uncertain initial conditions. Then, it can be shown [25] that the dependence of $f(\varepsilon)$ on ε is of type $f(\varepsilon) \propto \varepsilon^{\alpha}$, where $\alpha := N - D$ is the *uncertainty exponent* and D defines the uncertainty dimension. The uncertainty exponent α takes values between 0 (the boundary is totally fractal) and 1 (the boundary is a smooth curve). Note that this definition is consistent when we restrict to a submanifold $S \subset \mathbb{R}^N$ of dimension $N_0 < N$ (which is quite helpful for saving computational time): if we select initial conditions on S, the uncertainty dimension D is obtained from $D = D_0 + N - N_0$, where D_0 is the fractal dimension of the intersection between the fractal boundary and S, and is obtained from $\alpha = N_0 - D_0$.

In our computations, we fix $r_0 = 1.6$, $z_0 = 0$ and we take different values of $\theta_0 \in (\pi, 2\pi)$ (this values are suggested from Fig. 10 and 11). Therefore we have that $N_0 = 1$ and $N = 3$. Using this 1-dimensional submanifold we can obtain an uncertainty dimension D_0 that ranges from 0 to 1, and the uncertainty dimension of the system D verifies $D \in [2, 3]$. In particular, to approximate the uncertainty dimension D_0 we select an equispaced grid of M angles θ_i. The angle θ_i, for $i \in \{2, \ldots, M\}$, is certain if it escapes through the same exit as θ_{i-1}, and uncertain otherwise (by convention θ_1 is taken as certain). Note that in order to compute the exit point $r(t_{\text{escape}}) = R_{escape}$ we use a Newton method in a similar spirit to when computing a Poincaré map. We repeat these computations for $M = 100, 120, \ldots, (1.2)^n \cdot 100 < 10^6$ and we compute α from fitting linearly the expression $\log(f)$ versus $-\log(M)$. For example, in Fig. 12(b) we show one of the performed fits in order to stress that our computations are very accurate.

Figure 12(a) shows the fractal dimension obtained for system $\mathcal{C}$ (white squares) and system $\mathcal{C} + \mathcal{R}$ (black squares) as a function of the energy $H_0 > E_{\text{escape}}$, taking $L_0 = 4$. Let us first focus on system $\mathcal{C}$ to explain in some detail the main results of our numerical analysis.

1. We can see that it satisfies $D \to N = 3$ when $H_0 \to E_{\text{escape}}$. This is not surprising, as it was conjectured in [28] and fully explained in [4] that the fractal dimension of any open Hamiltonian system tends to that of phase space when the energy tends to the escape energy. In this limit, the size of the unique exit tends to zero, and the fractal basins become so fractalized that the boundary tends to fill up the whole phase space.

2. When the energy grows, the fractal dimension D decreases, as is usual in this kind of systems, and in the range $H_0 \in (E_{escape}, 1.195)$ the fractal dimension falls from 3 to 2.1. The fractality of system $\mathcal{C}$ strongly depends on the existence of its *Lyapunov orbit*:

an unstable periodic orbit that acts as the frontier of the scattering region, i.e. when a trajectory crosses it outwards the particle cannot enter the system again and escapes to infinity [14, 38]. At $H_0 = 1.195$ the Lyapunov orbit disappears and also its stable manifold, which in practice represents most of the fractal boundaries shown in Fig.10(a-c). Many systems similar to this one become smooth when their Lyapunov orbit vanishes, but for $H_0 > 1.195$ system $\mathcal{C}$ still shows very small fractalized regions that make the dimension be $D \approx 2.1$ for all values of the energy. This unexpected behaviour is due to the fact that for all energies there is another relevant unstable periodic orbit (of initial conditions $r_0 < 1$, $z_0 = 0$, $\theta_0 = 0$) on the invariant plane studied in Section 4.2. This orbit makes the trajectories that get close to it spend very long times in its vicinity before escaping to infinity.

3. Figure 13 shows some computations that clarify what we just explained in the previous item. In Fig. 13(a) we represent the escape time $t_{\rm escape}$ for a wide range of trajectories of system $\mathcal{C}$ and $H_0 = 1.18$ (solid line and a zoom in the inset figure), $H_0 = 1.20$ (dashed line) and $H_0 = 1.22$ (dotted-dashed line). For $H_0 = 1.18$ the system shows the expected pattern with multiple maxima that is a clear trace of fractality due to the existence of a chaotic saddle embedded in the system. Fig. 13(b) shows a typical chaotic trajectory in this regime: the particle spends some time following the Lyapunov orbit (plotted in the inset), then surrounds the invariant torus for some additional time and finally escapes from the system (note that, as already mentioned, the invariant torus exists for $H_0 \in (0.95, 1.21)$). For $H_0 = 1.20$ (dashed line) the Lyapunov orbit and all its fractality associated have disappeared, but the invariant torus remains; for this reason the escape time still shows a sharp maximum due to the trajectories that remain stuck to the torus for a long time before escaping. Finally, for $H_0 = 1.22$ (dotted-dashed line) the invariant torus has also disappeared and the escape time becomes totally smooth.

4. As we observed, however, the system shows certain complexity even for high values of the energy. Figure 13(c) shows the escape time $t_{\rm escape}$ for energy $H_0 = 2.5$, for which $D = 2.1$ and the footprint of some fractal behaviour can still be detected (see Fig. 10(d) for the corresponding exit basins). Figure 13(d) shows one example of a trajectory for this high value of the energy, and the inset shows the unstable periodic orbit responsible for all this uncertainty. Summarising, we conclude that there is not a chaotic saddle associated to this periodic orbit, and therefore this peculiar phenomenon detected for $H_0 > 1.195$ should be understood as a *spurious fractality*, more than the genuine fractal behaviour associated to chaotic scattering.

Let us finish with a few comments concerning system $\mathcal{C} + \mathcal{R}$. First of all let us note that it exhibits a dependence of the fractal dimension on the energy very similar to that of system $\mathcal{C}$ (see Fig. 12(a)). The reason is that for $L_0 = 4$ the influence of the rectilinear filament $\mathcal{R}$ on the scattering region is relatively weak in comparison to that of the circular wire $\mathcal{C}$. Lower

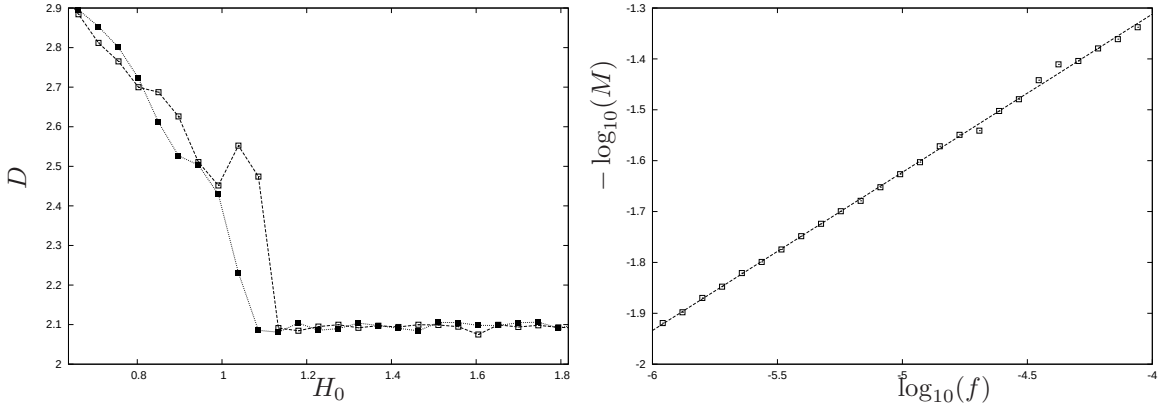

(a) Fractal dimension D versus energy H_0, where $H_0 \geq 0.64 \gtrsim E_{\text{escape}}$. White squares correspond to system $\mathcal{C}$ and black squares to system $\mathcal{C}+\mathcal{R}$.

(b) Illustration of the computation of $D = N - \alpha$, for $H_0 = 0.87364$, where α is the slope of $\log_{10}(f)$ versus $-\log_{10}(M)$.

Figure 12: Computation of fractal dimension D for systems $\mathcal{C}$ and $\mathcal{C}+\mathcal{R}$, when $L_0 = 4$. In this case $E_{\text{escape}} = 0.635247$.

values of L_0 show very different fractality between both systems, as happened with the fraction of stability when we studied bounded motions, cf. Fig. 8(a).

The destruction of fractality due to the disappearance of the fractal basins, however, is reached a bit sooner, for $H_0 = 1.182$, which means that system $\mathcal{C}$ is slightly more complex than system $\mathcal{C}+\mathcal{R}$ in this range of energies. Furthermore, the lack of the symmetry $(r, \theta) \to (r, \pi+\theta)$ makes the situation more difficult to analyse, as we cannot detect in system $\mathcal{C}+\mathcal{R}$ neither the Lyapunov orbit nor the unstable periodic orbit on the invariant plane that existed in system $\mathcal{C}$. We believe that other periodic orbits playing similar roles could exist for system $\mathcal{C}+\mathcal{R}$, but we have not been able to characterize them and to find the values of H_0 for which they appear. A satisfactory solution of this problem should involve an extension of the concept of Lyapunov orbit, which to the best of our knowledge has only been defined for natural Hamiltonian systems [14].

7 Conclusions and final remarks

In this paper we have studied the motion of a charged particle in the presence of a static, nonuniform magnetic field in three concrete examples: a straight line filament, a circular wire and a coupled system of both wires. In the first case, we have provided a complete analytical description of the motion, in particular, we have proved the existence of helicoidal trajectories. The case of the loop wire has been analysed both analytically and numerically, thus filling a gap in the literature. In particular we have proved the existence of periodic, quasi-periodic and scat-

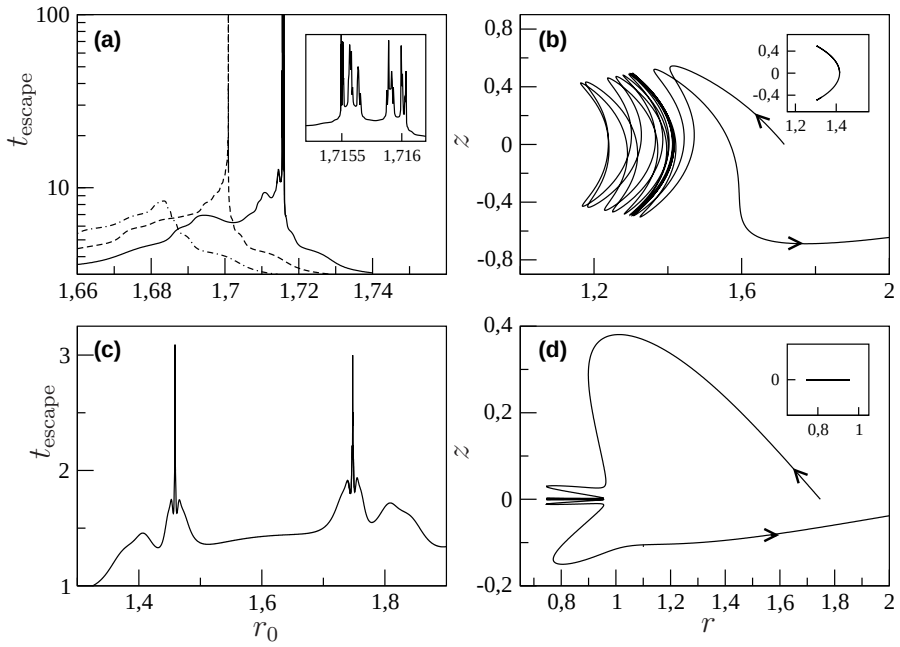

Figure 13: Analysis of the fractality of system $\mathcal{C}$ when H_0 is varied, for $L_0 = 4$. (a) Escape time $t_{\rm escape}$ for initial conditions (r_0 variable, $z_0 = 0$, $\theta_0 = 0.6\pi$) when $H_0 = 1.18$ (solid line), $H_0 = 1.20$ (dashed line) and $H_0 = 1.22$ (dotted-dashed line). The inset corresponds to $H_0 = 1.18$ and clearly shows its fractal nature. (b) Trajectory of a charge for $H_0 = 1.18$ corresponding to a maximum in (a). Inset: Lyapunov orbit for $H_0 = 1.18$. (c) Escape time $t_{\rm escape}$ for initial conditions (r_0 variable, $z_0 = 0$, $\theta_0 = 0.8\pi$) and $H_0 = 2.5$. (d) Trajectory of a charge for $H_0 = 2.5$ corresponding to one maximum in (c). Inset: Unstable periodic orbit responsible for spurious fractality at high energies.

tering trajectories, and, from the numerical viewpoint, we have provided evidences of chaotic scattering and Hamiltonian chaos. All these results can be interpreted in the context of plasma confinement since the circular wire is a toy model of the levitated magnetic dipole system. A similar study has been done for the coupled system, with the difference that the proof of existence of periodic and quasi-periodic motions has only been achieved assuming that the current intensity of the circular wire is much bigger than the current intensity of the infinite filament. Finally, we have explained how to construct a magnetic trap using the circular wire, which is based on our theoretical study of the confined motions in this system.

In spite of being a classical topic which is extremely important for applications, very few rigorous and global results on the motion of charges in magnetic fields are known. Specifically, for magnetic fields created by wires the guiding centre approximation does not provide reliable information for all times. This is illustrated with the examples of this paper, where the particle trajectories, the magnetic lines and the integral curves of $\nabla|B|$ have very little to do with each other. We would like to call the reader's attention to the following open problems.

Problem 7.1. *In Section 6, numerical evidence of Hamiltonian chaos, i.e. the presence of homoclinic tangles and positive Lyapunov exponents, is provided in the cases of the loop wire and the coupled system. It would be desirable to obtain a proof of this fact, which would be, to the best of our knowledge, the first rigorous verification of the existence of chaos for the motion of a charge in a magnetic field. A related question is to prove that there is not a third analytic first integral both for systems $\mathcal{C}$ and $\mathcal{C}+\mathcal{R}$.*

Problem 7.2. *We have proved in Section 3 that the equations of motion of a charge in an infinite rectilinear wire are Liouville integrable. We are not aware of other configurations of wires which give rise to integrable motions, so the problem that we pose is to prove that this is the only case which is Liouville integrable, at least in terms of analytic first integrals.*

Given an arbitrary current distribution, it is extremely difficult to obtain rigorous results on the motion of a charge in the magnetic field produced by this configuration. If the system has some Euclidean symmetry, as the examples discussed in this work, magnetic lines are not complicated, in particular they are not chaotic because they are organised according to a family of magnetic surfaces. Nevertheless, in this case the equations of motion possess a second first integral, which allows us to simplify the theoretical study, but the solutions can be very complicated, in fact chaotic, as numerically shown in Section 6. In particular, in this work we have compared a magnetic field having only periodic lines (system $\mathcal{C}$) with a magnetic field having periodic and quasi-periodic lines (system $\mathcal{C}+\mathcal{R}$) without obtaining significant differences in the motion of charged particles. In fact, system $\mathcal{C}$ seems to be more chaotic than system $\mathcal{C}+\mathcal{R}$ for some ranges of energy and some values of L_0. These observations raise the major questions:

Problem 7.3. *How complexity in magnetic lines is related to complexity in the motion? How the motion is related to the current filaments? Magnetic fields created by wires can be highly chaotic, cf. [3]. The more chaotic the field, the more chaotic the motion? How do regions ergodically filled by magnetic lines affect the trajectories of a charge? If we slightly perturb the circular wire we generally lose the axial symmetry, so we have to study a 3DOF Hamiltonian system. It is likely that many quasi-periodic motions are preserved provided that the perturbation is small enough, so we wonder whether this 3DOF system can exhibit Arnold's diffusion.*

We think that it is interesting to devote efforts to advance in these directions and we believe that a good understanding of this problem would give rise to interesting applications in different areas of research.

Acknowledgements

This work has been supported in part by the Spanish Ministry of Science under grants no. FIS05273-2008 (J.A.), MTM2006-00478 (A.L.) and MTM2007-62478 (D.P.-S.). The authors acknowledge the MICINN for financial support through a PhD scholarship FPU AP2005-2950

(A.L.) and the Juan de la Cierva program (D.P.-S.). We also acknowledge the use of EIXAM, the UPC Applied Math cluster system for research computing (see `http://www.ma1.upc.edu/eixam/`), in particular we are very grateful to P. Roldán for his support in the use of the cluster. We also appreciate motivating discussions with J.A. Jiménez, T.M. Seara and J. Villanueva.

References

[1] M. Abramowitz, I.A. Stegun, *Handbook of Mathematical Functions*. Dover, New York, 1965.

[2] J. Aguirre, J. Giné and D. Peralta-Salas, Integrability of magnetic fields created by current distributions. Nonlinearity 21 (2008) 51–69.

[3] J. Aguirre and D. Peralta-Salas, Realistic examples of chaotic magnetic fields created by wires. Europhys. Lett. 80 (2007) 60007.

[4] J. Aguirre and M.A.F. Sanjuán, Limit of small exits in open Hamiltonian systems. Phys. Rev. E 67 (2003) 056201.

[5] J. Aguirre, R. L. Viana and M. A. F. Sanjuán, Fractal structures in nonlinear dynamics. Rev. Mod. Phys. 81 (2009) 333–386.

[6] J. Berkowitz and C.S. Gardner, On the asymptotic series expansion of the motion of a charged particle in slowly varying fields. Comm. Pure Appl. Math. 12 (1959) 501–512.

[7] D. Biskamp, *Nonlinear Magnetohydrodynamics*. Cambridge Univ. Press, Cambridge, 1993.

[8] S. Bleher, C. Grebogi, and E. Ott, 'Bifurcation to chaotic scattering', Physica D **46**, 87–121 (1990).

[9] M. Braun, Particle motions in a magnetic field. J. Differential Equations 8 (1970) 294–332.

[10] L.S. Brown and G. Gabrielse, Geonium theory: physics of a single electron or ion in a Penning trap. Rev. Mod. Phys. 58 (1986) 233–311.

[11] K. Burns and G.P. Paternain, Anosov magnetic flows, critical values and topological entropy. Nonlinearity 15 (2002) 281–314.

[12] P. Caldirolli and M. Guida, Helicoidal trajectories of a charge in a nonconstant magnetic field. Adv. Diff. Eqs. 12 (2007) 601–622.

[13] C. Castilho, The motion of a charged particle on a Riemannian surface under a non-zero magnetic field. J. Differential Equations 171 (2001) 110–131.

[14] R.C. Churchill, G. Pecelli and D.L. Rod, Isolated unstable periodic orbits. J. Differential Equations 17 (1975) 329–348.

[15] J. Fortágh and C. Zimmermann, Magnetic microtraps for ultracold atoms. Rev. Mod. Phys. 79 (2007) 235–289.

[16] F. González-Gascón and D. Peralta-Salas, Invariant sets of second order differential equations. Phys. Lett. A 325 (2004) 340–354.

[17] F. González-Gascón and D. Peralta-Salas, Some properties of the magnetic fields generated by symmetric configurations of wires. Phys. D 206 (2005) 109–120.

[18] GSL-GNU Scientific library. `http://www.gnu.org/software/gsl/gsl.html`. Last update in 2008.

[19] E.M. Haacke, R.W. Brown, R. Venkatesan and M.R. Thompson, *Magnetic Resonance Imaging*. Wiley, New York (1999).

[20] M. Hénon and C. Heiles. The applicability of the third integral of motion: Some numerical experiments. Astronom. J. 69 (1964) 73–79.

[21] G.Z.K. Horvath, J.L. Hernández Pozos, K. Dholakia, J. Rink, D.M. Segal and R.C. Thompson, Ion dynamics in perturbed quadrupole ion traps, Phys. Rev. A 57 (1988) 1944–1956.

[22] J.D. Jackson, *Classical Electrodynamics*. Wiley, New York (1999).

[23] J. Kesner and M. Mauel, Plasma confinement in a levitated magnetic dipole. Plasma Phys. Rep. 23 (1997) 742–750.

[24] F. Kiessling, P. Nefzger and J. Nolasco, *Overhead Power Lines*. Springer, New York (2003).

[25] S.W. McDonald, C. Grebogi, E. Ott and J.A. Yorke, Fractal basin boundaries. Phys. D 17 (1985) 125–153.

[26] L. Michelotti, *Intermediate Classical Dynamics with Applications to Beam Physics*. Wiley, New York (1995).

[27] P.J. Morrison, Magnetic field lines, Hamiltonian dynamics, and nontwist systems. Phys. Plasmas 7 (2000) 2279–2289.

[28] A.P.S. de Moura and P.S. Letelier, Fractal basin boundaries in Hénon-Heiles and other polynomial potentials. Phys. Lett. A 256 (1999) 362–368.

[29] M. Muller, K. Dietrich, Classical motion of a charged particle in the magnetic field of a rectilinear current. Z. Phys. D 33 (1995) 101–107.

[30] T.G. Northrop, *The Adiabatic Motion of Charged Particles*. Interscience, New York (1963).

[31] D. Ostlie and B. Carroll, *An Introduction to Modern Stellar Astrophysics*. Addison-Wesley, Reading MA (1996).

[32] C.J.A. Pires et al., Magnetic field structure in the TCABR tokamak due to ergodic limiters with a non-uniform current distribution. Plasma Phys. Control. Fusion 47 (2005) 1609–1632.

[33] J. Reichel, Microchip traps and Bose-Einstein condensation. Appl. Phys. B 75 (2002) 469–487.

[34] J. Schmiedmayer, A wire trap for neutral atoms. Appl. Phys. B 60 (1995) 169–179.

[35] E.C. Silva, I.L. Caldas, R.L. Viana and M.A.F. Sanjuán, Escape patterns, magnetic footprints, and homoclinic tangles due to ergodic magnetic limiters. Phys. Plasmas 9 (2002) 4917–4928.

[36] C.L. Siegel and J.K. Moser. *Lectures on Celestial Mechanics*. Springer-Verlag, New York, 1971.

[37] C. Simó. Global dynamics and fast indicators. Global analysis of dynamical systems, 373–389, Inst. Phys., Bristol, 2001.

[38] C. Siopis, H.E. Kandrup, G. Contopoulos and R. Dvorak, Universal properties of escape in dynamical systems. Celest. Mech. Dyn. Astron. 65 (1997) 57–68.

[39] F. Truc, Trajectoires borneés d'une particule soumise á un champ magnétique symétrique linéaire. Ann. Inst. Henri Poincaré A 64 (1996) 127–154.

[40] R.K. Varma, Classical and macroquantum dynamics of charged particles in a magnetic field. Phys. Rep. 378 (2003) 301–434.

[41] G.E. Vekstein, N.A. Bobrova and S.V. Bulanov, On the motion of charged particles in a sheared force-free magnetic field. J. Plasma Phys. 67 (2002) 215–221.

[42] D. Yafaev, A particle in a magnetic field of an infinite rectilinear current. Math. Phys. Anal. Geom. 6 (2003) 219–230.

[43] A. Ynnerman, S.C. Chapman, M. Tsalas and G. Rowlands, Identification of symmetry breaking and a bifurcation sequence to chaos in single particle dynamics in magnetic reversals. Phys. D 139 (2000) 217–230.

[44] M. Yun and J. Yin, Controllable double-well magneto-optic atom trap with a circular current-carrying wire. Optics Lett. 30 (2005) 696–698.